Accepted Manuscript

The combination of quinazoline and chalcone moieties leads to novel potent heterodimeric modulators of Breast Cancer Resistance Protein (BCRP/ABCG2)

Stefanie Kraege, Katja Stefan, Kapil Juvale, Thomas Ross, Thomas Willmes, Michael Wiese

PII: S0223-5234(16)30249-5

DOI: 10.1016/j.ejmech.2016.03.067

Reference: EJMECH 8492

To appear in: *European Journal of Medicinal Chemistry*

Received Date: 17 December 2015

Revised Date: 8 March 2016

Accepted Date: 25 March 2016

Please cite this article as: S. Kraege, K. Stefan, K. Juvale, T. Ross, T. Willmes, M. Wiese, The combination of quinazoline and chalcone moieties leads to novel potent heterodimeric modulators of Breast Cancer Resistance Protein (BCRP/ABCG2), *European Journal of Medicinal Chemistry* (2016), doi: 10.1016/j.ejmech.2016.03.067.

The combination of quinazoline and chalcone moieties leads to novel potent heterodimeric modulators of Breast Cancer Resistance Protein (BCRP/ABCG2)

Stefanie Kraege,[‡] *Katja Stefan,*[‡] *Kapil Juvale, Thomas Ross, Thomas Willmes and Michael Wiese*[*]

Pharmaceutical Chemistry II, Pharmaceutical Institute, University of Bonn, An der Immenburg 4, 53121 Bonn, Germany

[‡] These authors contributed equally.

Keywords. ABC transporter, ABCG2, Multidrug resistance, Chalcones, Quinazolines, Quinazoline-chalcones, Pheophorbide A assay, ATPase

Abstract: During the last decade it has been found that chalcones and quinazolines are promising inhibitors of ABCG2. The combination of these two scaffolds offers a new class of heterocyclic compounds with potentially high inhibitory activity against ABCG2. For this purpose we investigated 22 different heterodimeric derivatives. In this series only methoxy groups were used as substituents as these had been proven superior for inhibitory activity of chalcones. All compounds were tested for their inhibitory activity, specificity and cytotoxicity. The most potent ABCG2 inhibitor in this series showed an IC_{50} value of 0.19 µM. It possesses low cytotoxicity (GI_{50} = 93 µM), the ability to reverse MDR and is nearly selective toward ABCG2. Most compounds containing dimethoxy groups showed slight activity against ABCB1 too. Among these three compounds (**17**, **19** and **24**) showed even higher activity toward ABCB1 than ABCG2. Selected inhibitors were further screened for their effect on basal ATPase activity. Although the basal ATPase activity was partially stimulated, the compounds were not transported by ABCG2. Thus, quinazoline-chalcones are a new class of effective ABCG2 inhibitors.

Introduction

Chemotherapy is one of the common treatments of cancer, but often fails due to the emergence of multidrug resistance (MDR). Often MDR is caused by overexpression of efflux transport proteins from the family of ATP-binding cassette (ABC) transporters.[1] Currently 48 members of ABC transporters are known in humans, which act as exporters and are divided into seven subfamilies. The typical ABC transporter consists of two nucleotide binding domains (NBDs) and two transmembrane domains (TMDs), containing six transmembrane helices each, as functional units. Hydrolysis of ATP yields the energy necessary for active transport and is performed by the NBDs. While most ABC transporters have specific substrates, some are polyspecific, recognizing a wide variety of structurally unrelated compounds. Three polyspecific ABC transporters, mostly associated with MDR in cancer, are ABCB1 (P-glycoprotein), ABCC1 (MRP1) and ABCG2 (BCRP).[2,3]

The most recently described polyspecific ABC transporter ABCG2 was first discovered in 1998 in the multidrug resistant breast cancer cell line MCF-7/AdrVp. It has a molecular weight of 72 kDa and consists of 655 amino acids.[4,5] ABCG2 contains only one NBD and one TMD and dimers or tetramers are considered to form the functional transporter.[6,7,8] The protein is the second member of the ABCG subfamily and is present in various organs with barrier functions, and is expressed in many types of cancer as well.[9] It is involved in MDR by transporting molecules with amphipathic characteristics, which can be neutral, positively or negatively charged. The structural diversity of substrates ranges from anticancer drugs such as mitoxantrone over various non-chemotherapy drugs to fluorescence dyes, like pheophorbide A.[10,11] The development of potent, selective and non-toxic inhibitors is one possibility to overcome MDR. A variety of compounds that can inhibit ABCG2 have been investigated during the last decade including fumitremorgin C (FTC), a highly potent and selective inhibitor produced by *Aspergillus fumigatus*, that is also highly neurotoxic.[12,13,14] Based on the scaffold of FTC the non-toxic inhibitor Ko143 was developed.[15] Tariquidar, a potent inhibitor

of ABCB1, has been shown to also inhibit ABCG2, though with lesser potency.[16] Derivatives lacking the tetrahydroisoquinoline moiety of tariquidar lost their ABCB1 inhibiting potency but retained their ABCG2 inhibition potential.[17,18,19,20] Naturally occurring flavonoids and derivatives have been described as potent inhibitors of ABCG2. [21,22,23,24] Also the investigation of their biochemical precursors, the chalcones and their derivatives as selective inhibitors of ABCG2 showed the possibility to overcome MDR *in vitro*. Chalcones were found to be potent ABCG2 inhibitors with IC_{50} values in the low micromolar range and the most potent derivative having an IC_{50} value of 0.53 µM in the Hoechst 33342 accumulation assay.[25] Nevertheless chalcones are limited in their maximum inhibitory potential. Quinazolines like the tyrosine kinase inhibitor gefitinib and structurally related derivatives are even more potent inhibitors of ABCG2 with IC_{50} values in the high nanomolar range.[26,27,28] In 2014 Winter et al.[29] developed a series of quinoxaline-substituted chalcones as new inhibitors of ABCG2. They replaced the ring B of the chalcone by a quinoxaline, a 2-napthyl or a 3,4-methylenedioxyphenyl residue and substituted ring A with varying methoxy group substitution patterns. In general the quinoxaline derivatives were found to be most potent and the presence of at least two methoxy groups on the A-ring is necessary for an effective inhibition of ABCG2. The most potent compounds possessed IC_{50} values in the low micromolar range in the mitoxanthrone efflux assay. Thus, the combination of two substructures of ABCG2 inhibitors provided more potent compounds. The benefit of combination of substructures was previously shown on the example of linked homodimers as modulators of ABCB1. In several cases an increase in the inhibitory potential of the compounds was observed.[30,31,32] Even strong potentiation of inhibitory activity was reported. For example, the galantamine dimer (Gal-2) inhibited ABCB1 efflux with an IC_{50} of 0.8 µM, while the monomer showed no inhibition up to 100 µM.[33]

Based on these results we decided to combine chalcones with quinazolines, in order to investigate whether there is also a benefit of combining both scaffolds of ABCG2 inhibitors.

Our decision was based on the available data regarding the binding region of chalcones and quinazolines. From the available literature data it can be concluded that both types of inhibitors most probably bind to the NBDs of ABC transporters and not to the common drug binding site located in the transmembrane domains. In case of quinazolines the possibility of attacking both binding sites exist as outlined below. For flavonoids, the successor of chalcones, several docking and 3D QSAR studies demonstrated that they target the nucleotide binding domain of ABCB1.[34,35,36] With regard to ABCG2 no detailed studies are available, but based on the highly conserved structure of the nucleotide binding domains, it is suggested that flavonoids inhibit similarly via interaction with the NBD.[37] Chalcones have not been investigated that intensively but they were shown to interact with the NBDs of ABCB1 by Bois et al.[38,39] Again nothing definite is known for ABCG2, but due to the conserved NBD structures, an analogous interaction can be assumed, as for flavonoids. This is corroborated by the finding that chalcones can interact with the ATP-binding site of tyrosine kinases, the targets of several quinazoline based TKIs.[40,41] Also structurally related dihydroxybenzophenones have been shown to bind to the NBD of ABCB1.[42] TKIs with quinazoline scaffold are known to bind to the ATP-binding site of the receptor tyrosine kinases.[43,44,45] Only a few quinazoline based TKIs have been investigated in detail for interaction with ABCB1 and ABCG2. While stimulation of ATPase activity was observed in submicromolar concentrations, replacement of radiolabelled [^{125}I] IAAP from ABCG2 membranes required much higher concentrations, or the compounds were not active at all.[46] Additionally Saito et al. demonstrated in kinetic analysis experiments that Gefitinib binds to an ABCG2-ATP complex.[47]

Therefore we designed and synthesized novel heterodimeric modulators based on the combination of chalcones with quinazolines, in order to investigate whether there is also a benefit of combining both scaffolds of ABCG2 inhibitors.

An amino linker at position 4 of the quinazoline moiety was used to couple the quinazolines with different substituted chalcones. Based on previous results from studies of both individual compound classes, 22 new derivatives were synthesized. Further modifications, like methoxy groups at position 6, 7 and the addition of a phenyl ring in position 2 of the quinazoline moiety, led to increased activity. The compounds were investigated for their inhibitory activity in MDCK II cells expressing ABCG2 using the pheophorbide A assay. ABCG2 selectivity was analyzed by screening for ABCB1 and ABCC1 inhibition using the calcein accumulation assay. Additionally, the compounds effect on basal ATPase activity was studied and enzyme kinetic measurements were performed to characterize the type of interaction with the substrate pheophorbide A.

Results and Discussion

Chemistry. The synthesis of the target compounds 17-38 is shown in Scheme 1.

First the quinazoline ring system was built by synthesizing quinazolinones. For this purpose two different methods, depending on the substitution in position 2 of the quinazolines, were used. For compounds without substitution at position 2 anthranilic acid or 2-amino-4,5-dimethoxybenzoic acid and excess formamide were reacted to yield compounds **1** and **2**. To obtain compounds **3** and **4** anthranilamide and an accordingly substituted benzaldehyde in dimethylformamide in presence of iodine and anhydrous potassium carbonate were reacted to yield the 2-substituted quinazolinones. Then chlorination with phosphoryl chloride produced the intermediates **5**-**8**. The substituted 4-chloroquinazolines were transformed into 4-anilinoquinazolines by reaction with 3- or 4-aminoacetophenones to produce the precursors **9**-**16**.[16] Finally, Claisen-Schmidt condensation of the ketones with different benzaldehydes, using LiOH as catalyst, led to the desired quinazoline-chalcones.[15] All synthesized compounds were characterized by NMR spectroscopy and the purity confirmed by LC-MS.

Biological Testing. Inhibition of ABCG2. The 22 synthesized quinazoline-chalcones were examined for their ability to inhibit ABCG2 using the pheophorbide A assay and the MDCK II BCRP cell line (Table 1). Pheophorbide A is a fluorescent breakdown product of chlorophyll and a well-known specific substrate of ABCG2.[11] The assay was performed as previously described with minor modifications.[48] Previous results from compounds with different substituents on ring B of the chalcone showed the necessity of a substituted phenyl ring. The unsubstituted derivatives were either inactive or showed only very low inhibitory activity, depending on the substitution pattern on ring A of the chalcone. From the investigated substituents methoxy substitution, especially 3,4-dimethoxy substitution, yielded the maximum inhibitory activity against ABCG2.[25] Compared to the quinazoline and chalcone building blocks the combination of both moieties generally led to increased activity. For example for the quinazoline 2-(3,4-dimethoxyphenyl)-4-anilinoquinazoline an IC_{50} value of 4.09 µM was reported[26] and for the chalcone (*E*)-1,3-Bis(3,4-dimethoxyphenyl)prop-2-en-1-one an IC_{50} of 5.12 µM.[49]

The first series of compounds (**17-26**) started with a *meta*-acryloylphenyl residue on ring A of the chalcone. All synthesized compounds showed an inhibitory effect against ABCG2 with IC_{50}-values in the range of 0.2 to 2 µM. Comparison of compounds **17** to **20** showed no significant differences related to methoxy substitution in positions 6 and 7 of the quinazoline moiety unsubstituted at position 2. Only the combination of 6,7-OCH_3 and 4'-OCH_3 on the chalcone residue leads to increased activity with compound **20** being most potent (IC_{50} = 0.32 µM). In both cases a 3',4'-dimethoxy substitution on ring B slightly decreased the inhibitory potency. This is in agreement with previous findings for 4-phenyl substituted quinazolines, where the additional methoxy groups at the quinazoline moiety had mostly an activity decreasing effect.[26]

Different results were obtained for quinazolines substituted at position 2 with a phenyl ring (**21-23**). The 3',4'-dimethoxy substitution was most potent, followed by the *meta*-substituted

methoxy derivative and the *para*-substituted analogue being the least active. If additional methoxy groups at the 2-phenyl ring were present (**24-26**) the activity pattern was identical to the unsubstituted quinazolines **17-20** (4'-methoxy substitution being superior to 3',4' disubstitution). In case of the quinazoline-chalcones there is still a positive effect of substituents at position 2 of the quinazoline moiety, but it is less pronounced as for the 2-phenyl substituted quinazolines without chalcone moitey.[26]

The second series of compounds (**27-38**) contained a *para*-acryloylphenyl residue on ring A of the chalcone. As before, compounds unsubstituted at position 2 of the quinazoline moiety, with or without methoxy groups on position 6 and 7 (**27-30**), were investigated. In this series the quinazoline-chalcones were substituted with methoxy groups in position 3' and 3',4' on ring B. Again the mono-substituted derivatives were more potent than their 3',4'-disubstituted counterparts. Comparing the *meta*-acryloyl with the *para*-acryloyl residues, the latter showed a slightly increased activity, compare **17** (IC_{50} = 1.30 µM) with **27** (IC_{50} = 0.84 µM) and **19** (IC_{50} = 1.71 µM) with **29** (IC_{50} = 1.23 µM). The two derivatives with 6,7-methoxy substitution and a single methoxy group at the chalcone ring B (**20** and **30**) possessed the highest inhibitory activity among the eight derivatives unsubstituted in position 2 of the quinazoline.

For the quinazoline chalcones **31-33** bearing a 2-phenyl ring the same effect of the substitution pattern was observed as for the *meta*-acryloyl derivatives **21-23**. Again the 3',4'-methoxy derivative **31** showed the highest activity (IC_{50} = 0.29 µM), while a 4'-methoxy group was detrimental (**33**: IC_{50} = 3.55 µM). As seen for the *meta*-acryloyl substituted compounds, a 3,4-dimethoxy substituted phenyl ring at position 2 of the quinazoline improved activity further in the series of *para*-acryloyl substituted derivatives. Compound **35** turned out to be the best in the whole series, with an IC_{50}-value of 0.19 µM only. But also the 3'-methoxy derivative **36** (IC_{50} = 0.36 µM) was nearly as potent as Ko143, the most potent ABCG2 inhibitor known so far. Interestingly the quinazoline-chalcones from both the *meta*

and *para* series without a substituent at ring B showed almost identical IC_{50}-values (**34**: 0.92 µM vs. **38**: 1.09 µM). A graphical summary of the effect of structural features of the quinazoline-chalcone scaffold for ABCG2 inhibition is given in Figure 1.

Taken together the comparisons of all synthesized quinazoline-chalcones, it can be concluded that compounds containing a *para*-acryloylphenyl residue are better inhibitors than those with a *meta*-acryloylphenyl residue and that the presence of 2-phenyl substitution at the quinazoline moiety leads to an increase in ABCG2 inhibition.

To examine the type of inhibition of quinazoline-chalcones enzyme kinetic studies were performed using the most potent compound 35 and pheophorbide A. The Lineweaver-Burk plot of the transport velocities for a range of substrate concentrations in absence or presence of various concentrations of compound **35** reveals that it is a non-competitive inhibitor of ABCG2 with regard to pheophorbide A, indicating that substrate and inhibitor have different binding sites (Figure 2).

Calcein accumulation assay to determine ABCB1 and ABCC1 inhibition. All synthesized compounds were additionally screened for their inhibition of ABCB1 and ABCC1 utilizing the calcein accumulation assay. The screening was conducted at a fixed concentration of 10 µM using A2780adr (ABCB1) and H69AR (ABCC1) cell lines. Cyclosporine A (10 µM) was used as standard inhibitor for both ABCB1 and ABCC1, respectively. Figure 3 illustrates the effects of the 22 quinazoline-chalcones on the accumulation of calcein and exemplifies that the studied substances possess higher affinity for ABCB1 (Figure 3A) than ABCC1 (Figure 3B). As could be expected, compounds with dimethoxy-substitution showed relatively high inhibition of ABCB1. Within the two series, the chalcones with *meta*-acryloylphenyl residue (**17-26)** were found to inhibit ABCB1 more than compounds with the *para*-acryloylphenyl residue (**27**-**38**). Concentration-response curves were generated for compounds showing more than 25 % inhibition at 10 µM. The results are depicted in Table 2 and reveal that three compounds **17** (IC_{50} = 0.42 µM), **19** (IC_{50} = 0.86 µM) and **24** (IC_{50} = 0.48 µM) have a

substantial ABCB1 inhibitory activity being mostly more active than in case of ABCG2. Therefore, these compounds represent dual inhibitors. Interestingly the dose-response curves of all compounds levelled off below the maximum fluorescence reached by cyclosporine A, pointing to the possibility of partial inhibition. Comparing the activities against both transporters the scatterplot shown in Figure 4 demonstrates that there is no correlation between the IC_{50} values for ABCG2 and ABCB1. The most potent ABCG2 inhibitor, **35** shows only a weak inhibition of ABCB1 function, no ABCC1 inhibition and can be classified as rather selective ABCG2 inhibitor.

Effects of quinazoline-chalcones on ATPase activity of ABCG2. To understand the interactions between quinazoline-chalcones and ABCG2 in more detail, we examined the effects of quinazoline-chalcones (1 µM) on the vanadate sensitive ATPase activity. As shown in Figure 5 most of the compounds lead to an increase of the ATPase activity. Additionally, compounds **27**, **31** and **35** activate the membrane ATPase nearly to the same extent as quercetin, a well-known potent activator of ABCG2 ATPase activity.[55] These compounds contain a *para*-acryloylphenyl residue linked to ring A and a 3,4-dimethoxy substitution at ring B of the chalcone. The data obtained suggest that quinazoline-chalcones act as ATPase activators and can be considered as substrates although the compounds were found to be inhibitors in the pheophorbide A accumulation assay. On the other hand compounds with two methoxy groups in positions 6 and 7 of the quinazoline scaffold (**19**, **20**, **29** and **30**) show an inhibiting or no effect on ABCG2 ATPase activity acting like Ko143 as inhibitors.

The effects of compound **30** (ATPase inhibiting compound) and **27, 35** (ATPase activating compounds) on ATPase activity were further characterized by determining concentration response curves (Figure 6). We observed that **35** increases ATPase activity up to a concentration of 1 µM followed by a decrease at higher concentrations. In contrast, compound **30** inhibits ATPase activity of ABCG2 up to 1 µM and showed no activating effect at higher concentrations.

The activation or inhibition of the ATPase is apparently influenced also by the scaffolds of the quinazoline-chalcones and depends on the concentration of the substances.

Investigation of compound 27 for its accumulation in ABCG2 overexpressing cells via primary fluorescence. The ability of quinazoline-chalcones to stimulate the ATPase of ABCG2 in nearly the same way as the standard substrate quercetin, supports the possibility that the compounds are transported by ABCG2.

Fluorescence microscopy was used to investigate this possibility. Among the ATPase stimulating derivatives compound **27** showed moderate fluorescence when excited at a wavelength of 405 nm and was selected for this investigation. Because of the similar excitation and emission wavelength of GFP (green fluorescent protein), linked to cDNA of ABCG2 transfected MDCK II cells, fluorescence studies were performed using parental MCF-7 and MCF-7 MX cells expressing ABCG2. Cells were incubated with compound **27** at 10 µM for 2 h, washed and cellular fluorescence was visualized using a Nikon A1 R confocal laser scanning microscope after 30 min. As it can be seen in Figure 7A and B, compound **27** showed no difference in fluorescence intensity between the wild-type MCF-7 and the ABCG2 overexpressing cell line MCF-7 MX, thus the efflux of the substance could be disproved. Our findings were confirmed by experiments in combination with the BCRP substrate pheophorbide A, showing its accumulation in resistant cell line MCF-7 MX in presence of compound **27** during the incubation time. Hereby, the fluorescence intensity was equal compared to the parental cell line MCF-7. Figure 7C-E highlight the results that the quinazoline-chalcones inhibit the transport of pheophorbide A but are not transported themselves.

Further kinetic studies were performed using fluorescence spectroscopy. Parental MCF-7 and MCF-7 MX cells were incubated with **27** for varying time intervals. After washing, the fluorescence of the cells was measured in a fluorimeter. The time-dependent determination of the intracellular fluorescence concentration for up to 3 h indicated that compound **27** behaved

in both cell lines in the same manner. Within the first minutes the intracellular concentration increases until reaching a plateau after approximately 60 min (Figure 8).

This is in agreement with the results from the confocal laser scanning microscopy disproving the assumption of transport of the quinazoline-chalcone by ABCG2. It seems that stimulation of the ATPase activity is not related to drug transport, e.g. behavior as a substrate.

Cytotoxicity of Quinazoline-chalcones. To eliminate cell specific effects and for determination of therapeutic ratios, all compounds were screened for their cytotoxic effects in the same MDCK II BCRP and MDCK II wild type cells. Cells were treated with a fixed concentration of 10 µM of the compounds. After 72 h incubation cell viability was determined using MTT colorimetric assay. As shown in Figure 9, most of the compounds have only low cytotoxic effects at a concentration of 10 µM. Only compounds **23**, **28**, **31** and **32** show high cytotoxicity, but no conclusion could be drawn with respect to their chemical structure. For the most potent representative of our compound set (**35**) complete dose response curves were generated. The result is in agreement with the screening, featuring no detectable cytotoxicity, with a GI_{50} value of about 93 µM (Figure 10). The ratios of IC_{50} values and GI_{50} values yield the therapeutic ratio (Table 3). Among the investigated derivatives compound **35** has the highest therapeutic ratio, pointing to its usability for further *in vivo* investigations. In comparison to this, the standard inhibitor Ko143 has a 10 fold lower therapeutic value due to its cytotoxicity.

Furthermore for selected compounds, which showed high inhibitory potencies towards ABCB1, we determined the cytotoxicity in A2780adr and parenteral A2780 cells additionally (Table 4). Compared to MDCK II cells all compounds were more toxic in A2780 parental and adr cells. When comparing the GI50-values of the compounds high intercorrelations become apparent (Table 5). Thus the compounds behave in all cell lines similar with varying baseline toxicity. As the cytotoxicities of the compounds in the wild type and the transporter containing cell lines do not differ significantly, it can be concluded that they are no or only

poor substrates of ABCG2 and ABCB1, in agreement with the results of the fluorescence measurements described above.

Quinazoline-chalcones potently reverse resistance to SN-38.

Furthermore, we checked the substances for their ability to reverse the multidrug resistance in ABCG2 overexpressing cells. For better comparison we also investigated the efficacy of Ko143, as known standard inhibitor of ABCG2. Compound **35**, which shows highest ABCG2 inhibition in the pheophorbide A accumulation assay as well as Ko143 were examined at final concentrations of 0.01 µM and 0.1 µM. Figure 11 depicts the shift in the dose response curves of the ABCG2 substrate SN-38, the active metabolite of irinotecan, (Figure 11A and B) in presence of the test compounds. These dose-response curves indicate an exceeding decrease in cell viability in ABCG2 overexpressing cells than in wild type cells. Compound **35** and Ko143 are able to partially reverse the ABCG2-mediated transport of SN-38 out of the cells, even at nanomolar concentrations.

Pharmacophore Search.

Matsson et al. reported in 2007 a minimum pharmacophore model for ABCG2 substrates.[50] It was derived from the effect of 123 diverse drugs or drug-like compounds on mitoxantrone efflux in Saos-2 cells transfected with human ABCG2. The pharmacophore model consists of two hydrophobic centers and one hydrogen bond acceptor feature. Together with lipophilicity as second descriptor, the pharmacophore model had a high discriminating power. More recently new pharmacophore models were generated by Ding et al.[51] These authors created a pharmacophore ensemble consisting of three different pharmacophores. For comparative purposes they merged parts from their pharmacophore models and found an agreement with the model of Matsson et al. Therefore it was of interest to investigate how well our compounds would fit to this pharmacophore model. The best compound **35** was used for

pharmacophore search. The three-point pharmacophore was built in MOE, the hydrophobic and hydrogen bond acceptor points defined and a pharmacophore search performed. Investigation of the matched conformations showed that basically two different overlays were found as shown in Figure 12.

In one alignment only the chalcone part was involved as shown in panel A of Figure 12. Although the fit is reasonable, it does not explain the gain in activity observed when combining quinazoline and chalcone substructures. The second alignment presented in panel B involves the 2-phenyl ring of the quinazoline part as hydrophobic center. The aromatic residue of the aniline linker, present in the quinazoline and chalcone substructure, is mapped on one of the hydrophobic centers. The acceptor feature is fulfilled by the carbonyl oxygen of the chalcone substructure. Again the pharmacophore fit cannot explain the observed SAR. The 2-phenyl ring is preferable, but not necessary for high activity as exemplified by compounds **18** and **20**, that belong to the most active derivatives. Also compounds **18** and **22** that differs only by the pharmacophoric 2-phenyl ring, possess almost identical potencies. Thus other structural motifs seem to be responsible for the activity differences within our series of compounds. This could be explained taken into account the assumption of binding of our derivatives to the NBD of ABCG2. The pharmacophore model of Matsson et al. was developed from drugs that almost exclusively are assumed to bind to the transmembrane region of ABCG2, distant from the NBD.

Conclusion

The combination of the quinazoline and chalcone inhibitors, leading to heterodimers yielded inhibitors with mostly IC_{50} values in the submicromolar range. Compared to the formal building blocks, the quinazoline 2-(3,4-dimethoxyphenyl)-4-anilinoquinazoline (IC_{50}: 4.09 µM) and the chalcone (*E*)-1,3-Bis(3,4-dimethoxyphenyl)prop-2-en-1-one (IC_{50}: 5.12 µM),

the best heterodimeric compound **35** (IC_{50}: 0.19 µM) showed 25 fold higher inhibitory potency against ABCG2.

As for quinazolines structural features like a 2-phenyl ring bearing two methoxy groups led to an increase of inhibitory activity. The majority of the substances showed low inhibition of ABCB1 and no activity against ABCC1. But three compounds (**17**, **19** and **24**) had higher potencies for ABCB1 than ABCG2. Compound **24**, as an example, was found to be a dual inhibitor with equal potencies for ABCG2 and ABCB1 (**24**: IC_{50}, ABCG2: 0.60 µM; IC_{50}, ABCB1: 0.48 µM). Due to the determined high cytotoxicity these compounds are limited in their therapeutic usage as dual inhibitors.

We further investigated the stimulation of ATPase activity and found most of the quinazoline-chalcones being ATPase activators, pointing to substrate properties despite their inhibitory activity in the pheophorbide A assay. Therefore we controlled, if the compounds were transported by ABCG2. Both experiments, laser scanning microscopy and fluorescence spectrometry, disproved the assumption of possible transport. For future work it will become more and more relevant to develop non-toxic compounds to inhibit the efflux function of ABC transporters and thus to increase the efficacy of chemotherapy in combination with anticancer drugs. Our compounds showed low cytotoxicity and the most potent ABCG2 inhibitor **35** had a GI_{50} value of about 93 µM. This compound was able to reverse MDR for the ABCG2 substrate SN-38 in the same concentration range and to the same extent as Ko143. The behavior of compound **35** in combination with conventional anticancer drugs in *vitro* and in *vivo* will be evaluated in further research. In summary, highly potent, partially selective and low toxic chalcone derivatives were developed that are able to overcome multidrug resistance in tumor cells.

EXPERIMENTAL SECTION

Chemistry. Materials. All utilized chemicals were purchased from Sigma-Aldrich, Acros Organics or Alfa Aesar and were used without further purification. During the synthesis reaction progress was monitored by thin layer chromatography (TLC) on aluminium sheets coated with silica gel 60 F_{254} (Merck). For microwave reactions, a CEM Discover-SP W/ACTIVENT Microwave was used. The structures of target compounds were approved by NMR and purity by LC-MS. NMR spectra were recorded on a Bruker Avance 500 MHz NMR spectrometer at 500 MHz (^{1}H) or 126 MHz (^{13}C) or Bruker Advance 600 MHz (^{1}H, 600MHz/^{13}C, 151MHz) NMR spectrometer. DMSO-d_6 was used as solvent at 303 K. The chemical shifts are reported as δ values (ppm) using the solvent peak as internal standard. Coupling constants *J* are given in Hertz and multiplicities of resonance signals are indicated as s (singlet), d (doublet), doublet of doublets (dd), triplet of doublets (td), t (triplet), doublet of triplets (dt), q (quartet) and m (multiplet). The ^{13}C signals were assigned with the aid of distortion less enhancement by polarization transfer (DEPT) and attached proton test (APT). The purity of final compounds were analyzed by ESI-mass spectra obtained on an LCMS instrument (Applied Biosystems API 2000 LCMS/MS, HPLC Agilent 1100). The purity of all target compounds was assigned to be ≥ 95 % by LC-MS.

Preparation of substituted quinazolin-4(3*H*)-ones.

Two different routes were applied for the synthesis of quinazolin-4(3H)-ones depending on presence or absence of the phenyl ring at position 2 of the quinazoline moiety. For the compounds bearing no substituent at position 2 method A was used, while for compounds with substitution at position 2 method B was employed.

Method A: To an amount of 1 eq. anthranilic acid or 2-amino-4,5-dimethoxybenzoic acid was added 4 eq. formamide and the reaction mixture was heated for 8-10 hours at 150 °C. Then, the mixture was cooled to room temperature and diluted with 50 ml water which resulted in the precipitation of solid. The precipitate was filtered and washed with water.

Quinazolin-4(3*H*)-one (1). Synthesized from anthranilic acid (0.033 mol, 4.5 g) and formamide (0.13 mol, 6g). The product was recrystallized from ethanol to yield white crystals (73 %).^{1}H NMR (500 MHz, DMSO-d_6) δ 12.20 (s, 1H), 8.13 – 8.10 (m, 1H), 8.07 (s, 1H), 7.82 – 7.78 (m, 1H), 7.65 (dd, *J* = 8.2, 0.6 Hz, 1H), 7.53 – 7.49 (m, 1H). ^{13}C NMR (126 MHz, DMSO-d_6) δ 160.88, 148.88, 145.52, 134.43, 127.32, 126.86, 125.96, 122.77.

6,7-Dimethoxyquinazolin-4(3*H*)-one (2). Synthesized from 2-amino-4,5-dimethoxybenzoic acid (5 mmol, 1 g) and formamide (20 mmol, 0.92 g). The product was recrystallized from ethanol to yield brown solid (48 %). ^{1}H NMR (500 MHz, DMSO-d_6) δ 12.02 (s, 1H), 7.96 (s, 1H), 7.43 (s, 1H), 7.12 (s, 1H), 3.89 (s, 3H), 3.86 (s, 3H). ^{13}C NMR (126 MHz, DMSO-d_6) δ 160.13, 154.58, 148.68, 144.99, 143.92, 115.73, 108.15, 105.08, 56.03, 55.81.

Method B: To a solution of 20 mmol anthranilamide and 20 mmol substituted benzaldehyde in DMF (20 ml) were added 25 mmol iodine and 20 mmol anhydrous potassium carbonate. Then, the mixture was stirred under for 4-5 hours at 90 °C. After the completion of the reaction, the mixture was poured on to crushed ice resulting in a precipitation of solid. The

precipitate was filtered and washed with 100 ml 20% solution of sodium thiosulfate, to remove residual iodine, and finally with water.

2-Phenylquinazoline-4(3*H*)-one (3). Synthesized from anthranilamide and benzaldehyde. The product was recrystallized from ethanol to yield pale yellow solid (71 %). ^{1}H NMR (500 MHz, DMSO-d_6) δ 12.41 (s, 1H), 8.19 – 8.17 (m, 2H), 8.15 (dd, *J* = 7.9, 1.6 Hz, 1H), 7.85 – 7.80 (m, 1H), 7.75 – 7.71 (m, 1H), 7.58 – 7.56 (m, 1H), 7.56 – 7.52 (m, 2H), 7.51 – 7.49 (m, 1H). ^{13}C NMR (126 MHz, DMSO-d_6) δ 162.55, 152.64, 148.85, 134.64, 133.00, 131.46, 128.70 (2C), 127.89 (2C), 127.52, 126.63, 125.98, 121.13.

2-(3,4-Dimethoxyphenyl)quinazolin-4(3*H*)-one (4). Synthesized from anthranilamide and 3,4-dimethoxybenzaldehyde. The product was recrystallized from ethanol to yield pale brown solid (44 %). ^{1}H NMR (500 MHz, DMSO-d_6) δ 12.32 (s, 1H), 8.12 (dd, *J* = 8.1, 1.3 Hz, 1H), 7.87 (dd, *J* = 8.5, 2.2 Hz, 1H), 7.81 (d, *J* = 2.2 Hz, 1H), 7.80 – 7.77 (m, 1H), 7.70 (dd, *J* = 8.1, 0.5 Hz, 1H), 7.49 – 7.44 (m, 1H), 7.10 (dd, *J* = 8.2, 4.0 Hz, 1H), 3.88 (s, 3H), 3.84 (s, 3H). ^{13}C NMR (126 MHz, DMSO-d_6) δ 162.67, 152.17, 151.72, 149.01, 148.70, 134.58, 127.32, 126.17, 125.96, 125.05, 121.29, 120.83, 111.55, 110.92, 55.84, 55.83.

General procedure for the Preparation of substituted 4-chloroquinazolines (5-8). The selected quinazolin-4(3*H*)-one (10 mmol) was mixed with 10 ml phosphoryl chloride and was then stirred under reflux for 9 hours. After completion of the reaction the solvent was evaporated under reduced pressure. Ice-water was added to the residue and the formed precipitate was neutralized with ammonium hydroxide and was filtered off.

4-Chloroquinazoline (5). The product was synthesized from compound **(1)** and recrystallized from ethanol to yield pale yellow solid (50 %). ^{1}H NMR (500 MHz, DMSO-d_6) δ 8.62 (s, 1H), 8.17 – 8.12 (m, 1H), 7.91 – 7.86 (m, 1H), 7.78 (d, *J* = 8.2 Hz, 1H), 7.63 – 7.57 (m, 1H). ^{13}C NMR (126 MHz, DMSO-d_6) δ 160.01, 147.16, 144.23, 135.22, 127.85, 126.40, 124.24, 122.02.

4-Chloro-6,7-dimethoxyquinazoline (6). The product was synthesized from compound **(2)** and recrystallized from ethanol to yield pale yellow solid (64 %). ^{1}H NMR (500 MHz, DMSO-d_6) δ 8.86 (s, 1H), 7.42 (s, 1H), 7.36 (s, 1H), 4.00 (s, 3H), 3.98 (s, 3H). ^{13}C NMR (126 MHz, DMSO-d_6) δ 158.00, 156.88, 152.31, 151.53, 148.72, 118.72, 107.00, 102.37, 56.65, 56.30.

4-Chloro-2-phenylquinazoline (7). The product was synthesized from compound **(3)** and recrystallized from ethanol to yield brown solid (68 %). ^{1}H NMR (500 MHz, DMSO-d_6) δ 8.19 – 8.12 (m, 3H), 7.90 – 7.85 (m, 2H), 7.67 – 7.62 (m, 1H), 7.61 – 7.55 (m, 3H). ^{13}C NMR (126 MHz, DMSO-d_6) δ 161.80, 153.93, 146.17, 135.15, 132.29, 131.09, 128.78, 128.50, 127.31, 126.21, 125.70, 120.75.

4-Chloro-2-(3,4-dimethoxyphenyl)quinazoline (8). The product was synthesized from compound **(4)** and recrystallized from ethanol to yield brown solid (91 %). ^{1}H NMR (500 MHz, DMSO-d_6) δ 8.22 (dt, *J* = 8.3, 0.9 Hz, 1H), 8.09 (dd, *J* = 8.5, 2.0 Hz, 1H), 8.06 (d, *J* = 3.5 Hz, 2H), 8.00 (d, *J* = 2.0 Hz, 1H), 7.79 – 7.75 (m, 1H), 7.13 (d, *J* = 8.5 Hz, 1H), 3.89 (s, 3H), 3.85 (s, 3H). ^{13}C NMR (126 MHz, DMSO-d_6) δ 161.79, 158.95, 152.05, 151.43, 149.03, 135.91, 128.86, 128.60, 128.41, 125.74, 122.11, 121.55, 111.75, 110.97, 55.80, 55.71.

General procedure for the preparation of 4-anilinoquinazolines (9-16). A mixture of substituted 4-chloroquinazoline (2 mmol) and 3- or 4-aminoacetophenone (2 mmol) was dissolved in hot 2-propanol (25 ml) and refluxed for 1-2 hours. After completion of the reaction the formed precipitate was filtered off and washed with 2-propanol (15 ml). The product was recrystallized from ethanol.

1-(4-(quinazolin-4-ylamino)phenyl)ethanone (9). The product was synthesized from 4-chloroquinazoline (**5**) (1.9 mmol, 312 mg) and 4-aminoacetophenone (1.9 mmol, 256 mg) to yield pale yellow solid (58 %). ^{1}H NMR (500 MHz, DMSO-d_6) δ 11.92 (s, 1H), 9.06 (d, *J* = 8.3 Hz, 1H), 8.99 (s, 1H), 8.14 – 8.09 (m, 1H), 8.09 – 8.03 (m, 3H), 8.01 – 7.97 (m, 2H), 7.90 – 7.85 (m, 1H), 2.60 (s, 3H). ^{13}C NMR (126 MHz, DMSO-d_6) δ 197.05, 160.04, 151.20,

141.30, 139.39, 136.45, 134.47, 130.61, 129.00 (2C), 128.81, 125.23, 124.30, 120.23, 113.95, 26.83.

1-(3-(quinazolin-4-ylamino)phenyl)ethanone (10). The product was synthesized from 4-chloroquinazoline (**5**) (1.9 mmol, 312 mg) and 3-aminoacetophenone (1.9 mmol, 256 mg) to yield pale yellow solid (49 %) ^{1}H NMR (500 MHz, DMSO-d_6) δ 11.98 (s, 1H), 9.04 (d, *J* = 8.1 Hz, 1H), 8.95 (s, 1H), 8.32 (t, *J* = 1.8 Hz, 1H), 8.14 – 8.09 (m, 1H), 8.08 – 8.01 (m, 2H), 7.94 – 7.91 (m, 1H), 7.89 – 7.85 (m, 1H), 7.64 (t, *J* = 7.9 Hz, 1H), 2.61 (s, 3H). ^{13}C NMR (126 MHz, DMSO-d_6) δ 197.49, 160.18, 151.17, 138.96, 137.49, 137.35, 136.42, 129.51, 129.30, 128.79, 126.60, 125.16, 124.34, 119.95, 113.71, 26.95.

1-(4-((6,7-dimethoxyquinazolin-4-yl)amino)phenyl)ethanone (11). The product was synthesized from 4-chloro-6,7-dimethoxyquinazoline (**6**) (1.25 mmol, 280 mg) and 4-aminoacetophenone (1.25 mmol, 168 mg) to yield pale yellow solid (94 %). ^{1}H NMR (500 MHz, DMSO-d_6) δ 11.65 (s, 1H), 8.87 (s, 1H), 8.46 (s, 1H), 8.04 – 8.01 (m, 2H), 7.98 – 7.94 (m, 2H), 7.41 (s, 1H), 4.03 (s, 3H), 3.98 (s, 3H), 2.59 (s, 3H). ^{13}C NMR (126 MHz, DMSO-d_6) δ 196.95, 158.11, 156.58, 150.42, 148.66, 141.64, 136.19, 133.99, 128.88 (2C), 124.03 (2C), 107.81, 104.37, 99.96, 57.26, 56.59, 26.74

1-(3-((6,7-dimethoxyquinazolin-4-yl)amino)phenyl)ethanone (12). The product was synthesized from 4-chloro-6,7-dimethoxyquinazoline (**6**) (2.5 mmol, 561 mg) and 3-aminoacetophenone (2.5 mmol, 338 mg) to yield white solid (94 %). ^{1}H NMR (500 MHz, DMSO-d_6) δ 11.61 (s, 1H), 8.83 (s, 1H), 8.41 (s, 1H), 8.27 (t, *J* = 1.8 Hz, 1H), 8.06 – 8.01 (m, 1H), 7.91 – 7.87 (m, 1H), 7.62 (t, *J* = 7.9 Hz, 1H), 7.39 (s, 1H), 4.03 (s, 3H), 3.99 (s, 3H), 2.61 (s, 3H). ^{13}C NMR (126 MHz, DMSO-d_6) δ 197.57, 158.36, 156.53, 150.41, 148.82, 137.65, 137.45, 135.90, 129.41, 129.22, 126.20, 124.09, 107.52, 104.28, 99.96, 57.19, 56.61, 26.95.

1-(4-((2-phenylquinazolin-4-yl)amino)phenyl)ethanone (13). The product was synthesized from 4-chloro-2-phenylquinazoline (**7**) (9 mmol, 2.2 g) and 4-aminoacetophenone (9 mmol,

1.2 g) to yield yellow solid (88 %). ^{1}H NMR (500 MHz, DMSO-d_6) δ 11.50 (s, 1H), 8.95 (d, *J* = 8.2 Hz, 1H), 8.45 – 8.41 (m, 2H), 8.31 (d, *J* = 8.2 Hz, 1H), 8.11 (s, 4H), 8.08 (t, *J* = 7.7 Hz, 1H), 7.81 (t, *J* = 7.5 Hz, 1H), 7.69 (t, *J* = 7.1 Hz, 1H), 7.63 (t, *J* = 7.4 Hz, 2H), 2.62 (s, 3H). ^{13}C NMR (126 MHz, DMSO-d_6) δ 197.01, 159.05, 157.78, 141.98, 135.81 (2C), 133.84, 133.00, 129.23 (2C), 129.13 (4C), 128.05, 124.62, 123.41 (2C), 113.31, 26.79. Two quaternary C atoms are missing.

1-(3-((2-phenylquinazolin-4-yl)amino)phenyl)ethanone (14). The product was synthesized from 4-chloro-2-phenylquinazoline (**7**) (1 mmol, 240 mg) and 3-aminoacetophenone (1 mmol, 135 mg) to yield yellow solid (88 %). ^{1}H NMR (500 MHz, DMSO-d_6) δ 11.68 (s, 1H), 8.97 (d, *J* = 8.2 Hz, 1H), 8.59 (s, 1H), 8.44 (d, *J* = 7.3 Hz, 2H), 8.37 (d, *J* = 8.3 Hz, 1H), 8.15 (dd, *J* = 8.0, 1.3 Hz, 1H), 8.08 (t, *J* = 7.6 Hz, 1H), 7.92 (d, *J* = 7.8 Hz, 1H), 7.82 (t, *J* = 7.6 Hz, 1H), 7.71 – 7.65 (m, 2H), 7.61 (t, *J* = 7.6 Hz, 2H), 2.63 (s, 3H). ^{13}C NMR (126 MHz, DMSO-d_6) δ 197.58, 159.12 (2C), 157.51, 137.83, 137.40 (2C), 135.90, 133.24, 129.34 (2C), 129.23 (2C), 129.06 (2C), 128.66, 128.14, 126.01, 124.66, 123.61, 113.03, 26.94.

1-(4-((2-(3,4-dimethoxyphenyl)quinazolin-4-yl)amino)phenyl)ethanone (15). Synthesized from 4-chloro-2-(3,4-dimethoxyphenyl)quinazoline (8) (1.2 mmol, 360 mg) and 4-aminoacetophenone (1.2 mmol, 162 mg) to yield yellow solid (86 %). ^{1}H NMR (500 MHz, DMSO-d6) δ 11.58 (s, 1H), 8.88 (d, *J* = 8.3 Hz, 1H), 8.46 (d, *J* = 8.0 Hz, 1H), 8.14 – 8.11 (m, 2H), 8.10 – 8.07 (m, 2H), 8.07 – 8.03 (m, 3H), 7.77 (t, *J* = 7.6 Hz, 1H), 7.20 – 7.17 (m, 1H), 3.88 (s, 3H), 3.87 (s, 3H), 2.61 (s, 3H). ^{13}C NMR (126 MHz, DMSO) δ 197.00, 158.72, 156.64, 153.55, 148.88, 141.67, 135.96 (2C), 134.12, 128.98, 128.93 (2C), 127.87, 124.67, 123.93, 123.78, 112.78, 112.17, 111.82, 56.04, 55.97, 26.80. Two quaternary C atoms are missing.

1-(3-((2-(3,4-dimethoxyphenyl)quinazolin-4-yl)amino)phenyl)ethanone (16). Synthesized from 4-chloro-2-(3,4-dimethoxyphenyl)quinazoline (8) (0.67 mmol, 200 mg) and 3-aminoacetophenone (0.67 mmol, 91 mg) to yield yellow solid (88 %). ^{1}H NMR (500 MHz,

DMSO-d6) δ 11.48 (s, 1H), 8.82 (d, *J* = 8.1 Hz, 1H), 8.46 (s, 1H), 8.36 (d, *J* = 8.1 Hz, 1H), 8.14 (d, *J* = 7.8 Hz, 1H), 8.11 (dd, *J* = 8.5, 2.0 Hz, 1H), 8.07 (t, J = 7.6 Hz, 1H), 8.04 (d, *J* = 2.1 Hz, 1H), 7.94 (d, *J* = 7.7 Hz, 1H), 7.79 (t, *J* = 7.7 Hz, 1H), 7.69 (t, *J* = 7.9 Hz, 1H), 7.19 (d, *J* = 8.6 Hz, 1H), 3.88 (s, 3H), 3.83 (s, 3H), 2.64 (s, 3H). ^{13}C NMR (126 MHz, DMSO-d_6) δ 197.63, 158.85, 156.67, 153.60, 148.89, 137.69, 137.40, 135.93, 129.16, 129.09, 127.89, 126.29, 124.63, 123.86, 123.80, 112.64, 112.20, 111.72, 56.06, 55.99, 26.97. Two quaternary C atoms are missing.

Preparation of quinazoline-chalcones. General procedure for synthesis of compound 17-38. A mixture of 1 eq. 4-anilinoquinazoline, 1eq. substituted benzaldehyde and 7 eq. lithium hydroxide in 5 ml methanol was stirred under microwave irradiation (120W, 100°C) for 30 minutes. After completion of the reaction the solution was acidified with diluted hydrochloric acid. Then the solvent was evaporated under reduced pressure and the product was recrystallized from ethanol/water (1:1).

(E)-3-(3,4-dimethoxyphenyl)-1-(3-(quinazolin-4-ylamino)phenyl)prop-2-en-1-one (17). The product was synthesized from 1-(3-(quinazolin-4-ylamino)phenyl)ethanone (**10**) and 3,4-dimethoxybenzaldehyde to yield yellow solid (34 %). ^{1}H NMR (500 MHz, DMSO-d_6) δ 11.87 (s, 1H), 9.00 (d, *J* = 8.1 Hz, 1H), 8.96 (s, 1H), 8.47 (t, *J* = 1.8 Hz, 1H), 8.15 – 8.12 (m, 2H), 8.10 (dd, *J* = 8.8, 1.1 Hz, 1H), 8.00 (d, *J* = 7.9 Hz, 1H), 7.91 – 7.87 (m, 1H), 7.82 (d, *J* = 15.5 Hz, 1H), 7.75 (d, *J* = 15.5 Hz, 1H), 7.70 (t, *J* = 7.9 Hz, 1H), 7.54 (d, *J* = 1.9 Hz, 1H), 7.41 (dd, *J* = 8.4, 1.9 Hz, 1H), 7.03 (d, *J* = 8.4 Hz, 1H), 3.86 (s, 3H), 3.82 (s, 3H). ^{13}C NMR (126 MHz, DMSO-d_6) δ 188.66, 160.11, 151.63, 151.38, 149.22, 145.18, 139.32, 138.60, 137.51, 136.38, 129.35, 129.14, 128.80, 127.56, 126.72, 125.00, 124.63, 124.18, 120.27, 119.67, 113.77, 111.80, 111.14, 55.99, 55.80. LC-MS (*m/z*): positive mode 412 $[M+H]^+$. Purity by HPLC-UV (254 nm)-ESI-MS: 96 %.

(E)-3-(4-methoxyphenyl)-1-(3-(quinazolin-4-ylamino)phenyl)prop-2-en-1-one (18).

The product was synthesized from 1-(3-(quinazolin-4-ylamino)phenyl)ethanone (**10**) and 4-methoxybenzaldehyde to yield ochre solid (33 %). ^{1}H NMR (500 MHz, DMSO-d_6) δ 11.94 (s, 1H), 9.02 (d, *J* = 8.3 Hz, 1H), 8.97 (s, 1H), 8.46 (t, *J* = 1.8 Hz, 1H), 8.15 – 8.10 (m, 2H), 8.09 – 8.05 (m, 1H), 8.02 (d, *J* = 7.7 Hz, 1H), 7.91 – 7.88 (m, 1H), 7.87 – 7.84 (m, 2H), 7.77 (d, *J* = 3.0 Hz, 2H), 7.69 (t, *J* = 7.9 Hz, 1H), 7.04 – 6.99 (m, 2H), 3.82 (s, 3H). ^{13}C NMR (126 MHz, DMSO-d_6) δ 188.58, 161.67, 160.18, 151.26, 144.65, 139.04, 138.56, 137.43, 136.43, 131.02 (2C), 129.38, 129.26, 128.81, 127.36, 126.73, 125.07, 124.81, 120.05, 119.54, 114.60 (2C), 113.72, 55.56. LC-MS (m/z): positive mode 382 $[M+H]^+$. Purity by HPLC-UV (254 nm)-ESI-MS: 98 %.

(E)-3-(3,4-dimethoxyphenyl)-1-(3-((6,7-dimethoxyquinazolin-4-yl)amino)phenyl) prop-2-en-1-one (19). The product was synthesized from 1-(3-((6,7-dimethoxyquinazolin-4-yl)amino)phenyl)ethanone (**12**) and 3,4-dimethoxybenzaldehyde to yield yellow solid (30 %). ^{1}H NMR (500 MHz, DMSO-d_6) δ 9.66 (s, 1H), 8.49 (s, 1H), 8.37 (t, *J* = 1.9 Hz, 1H), 8.28 – 8.24 (m, 1H), 7.95 – 7.93 (m, 1H), 7.89 (s, 1H), 7.80 (d, *J* = 15.5 Hz, 1H), 7.74 (d, *J* = 15.5 Hz, 1H), 7.59 (t, *J* = 7.9 Hz, 1H), 7.53 (d, *J* = 2.0 Hz, 1H), 7.40 (dd, *J* = 8.4, 2.0 Hz, 1H), 7.20 (s, *J* = 1.9 Hz, 1H), 7.03 (d, *J* = 8.4 Hz, 1H), 3.98 (s, 3H), 3.94 (s, 3H), 3.85 (s, 3H), 3.82 (s, 3H). ^{13}C NMR (126 MHz, DMSO-d_6) δ 189.23, 156.45, 154.52, 152.89, 151.53, 149.22, 149.16, 147.26, 144.83, 140.27, 138.44, 128.92, 127.66, 126.77, 124.03, 123.71, 121.63, 119.96, 111.81, 111.11, 109.09, 107.39, 102.05, 56.40, 55.99, 55.92, 55.79. LC-MS (*m/z*): positive mode 472 $[M+H]^+$. Purity by HPLC-UV (254 nm)-ESI-MS: 99 %.

(E)-1-(3-((6,7-dimethoxyquinazolin-4-yl)amino)phenyl)-3-(4-methoxyphenyl)prop-2-en-1-one (20). The product was synthesized from 1-(3-((6,7-dimethoxyquinazolin-4-yl)amino)phenyl)ethanone (**12**) and 4-methoxybenzaldehyde to yield pale yellow solid (13 %).^{1}H NMR (500 MHz, DMSO-d_6) δ 9.65 (s, 1H), 8.49 (s, 1H), 8.37 (s, 1H), 8.25 (dd, *J* = 8.0, 1.6 Hz, 1H), 7.92 (d, *J* = 7.7 Hz, 1H), 7.89 – 7.83 (m, 3H), 7.76 (d, *J* = 1.6 Hz, 2H), 7.58 (t, *J* = 7.9 Hz, 1H), 7.20 (s, 1H), 7.02 (d, *J* = 8.8 Hz, 2H), 3.98 (s, 3H), 3.94 (s, 3H), 3.82 (s,

3H). ^{13}C NMR (126 MHz, DMSO-d_6) δ 189.15, 161.58, 156.43, 154.51, 152.89, 149.15, 147.25, 144.29, 140.25, 138.39, 130.93 (2C), 128.94, 127.44, 126.76, 123.62, 121.64, 119.82, 114.61 (2C), 109.07, 107.38, 102.03, 56.39, 55.98, 55.54. LC-MS (*m/z*): positive mode 442 $[M+H]^+$. Purity by HPLC-UV (254 nm)-ESI-MS: 99 %.

(E)-3-(3,4-dimethoxyphenyl)-1-(3-((2-phenylquinazolin-4-yl)amino)phenyl)prop-2-en-1-one (21). The product was synthesized from 1-(3-((2-phenylquinazolin-4-yl)amino)phenyl)ethanone (**14**) and 3,4-dimethoxybenzaldehyde to yield yellow solid (34 %). ^{1}H NMR (500 MHz, DMSO-d_6) δ 11.53 (s, 1H), 8.94 (d, *J* = 7.6 Hz, 1H), 8.77 (s, 1H), 8.44 (d, *J* = 7.4 Hz, 2H), 8.28 (d, *J* = 6.6 Hz, 1H), 8.21 – 8.17 (m, 1H), 8.14 – 8.05 (m, 2H), 7.88 – 7.81 (m, 2H), 7.78 (d, *J* = 15.5 Hz, 1H), 7.73 (t, *J* = 7.9 Hz, 1H), 7.63 (t, *J* = 7.2 Hz, 1H), 7.56 (t, *J* = 7.6 Hz, 2H), 7.49 (d, *J* = 1.9 Hz, 1H), 7.37 (dd, *J* = 8.3, 1.8 Hz, 1H), 7.00 (d, *J* = 8.4 Hz, 1H), 3.81 (s, 3H), 3.78 (s, 3H). ^{13}C NMR (126 MHz, DMSO-d_6) δ 188.76, 159.07, 157.78, 151.58, 149.18 (2C), 145.05, 138.48, 138.16, 138.11, 135.69, 129.28 (2C), 129.14 (2C), 129.03 (2C), 128.15, 128.02, 127.58, 125.93, 124.46, 124.13 (2C), 123.89, 119.66 (2C), 113.18, 111.77, 111.07, 55.87, 55.79. LC-MS (*m/z*): positive mode 488 $[M+H]^+$. Purity by HPLC-UV (254 nm)-ESI-MS: 96 %.

(E)-3-(4-methoxyphenyl)-1-(3-((2-phenylquinazolin-4-yl)amino)phenyl)prop-2-en-1-one (22). The product was synthesized from 1-(3-((2-phenylquinazolin-4-yl)amino)phenyl)ethanone (**14**) and 4-methoxybenzaldehyde to yield yellow solid (22 %).^{1}H NMR (500 MHz, DMSO-d_6) δ 10.06 (s, 1H), 8.82 (t, *J* = 1.8 Hz, 1H), 8.62 (d, *J* = 8.2 Hz, 1H), 8.52 – 8.48 (m, 2H), 8.26 (dd, *J* = 8.1, 1.4 Hz, 1H), 7.96 (d, *J* = 8.1 Hz, 1H), 7.90 – 7.88 (m, 2H), 7.82 – 7.78 (m, 4H), 7.68 – 7.66 (m, 1H), 7.66 – 7.62 (m, 1H), 7.48 – 7.44 (m, 3H), 6.99 (d, *J* = 8.8 Hz, 2H), 3.81 (s, 3H). ^{13}C NMR (126 MHz, DMSO-d_6) δ 189.16, 161.55, 159.15, 158.05, 150.70, 144.24, 140.07, 138.45, 138.39, 133.50, 130.88 (2C), 130.43, 129.05, 128.55 (2C), 128.34, 128.09 (2C), 127.44, 126.32, 126.23, 123.76, 123.18, 121.81, 119.82,

114.57 (2C), 114.16, 55.54. LC-MS (*m/z*): positive mode 458 $[M+H]^+$. Purity by HPLC-UV (254 nm)-ESI-MS: 95 %.

(E)-3-(3-methoxyphenyl)-1-(3-((2-phenylquinazolin-4-yl)amino)phenyl)prop-2-en-1-one (23). The product was synthesized from 1-(3-((2-phenylquinazolin-4-yl)amino)phenyl)ethanone (**14**) and 3-methoxybenzaldehyde to yield ochre solid (48 %). ^{1}H NMR (500 MHz, DMSO-d_6) δ 11.62 (s, 1H), 8.97 (d, *J* = 8.1 Hz, 1H), 8.78 (s, 1H), 8.44 (d, *J* = 7.3 Hz, 2H), 8.32 (d, *J* = 7.6 Hz, 1H), 8.20 (dd, *J* = 7.91, 1.3 Hz, H), 8.13 (d, *J* = 7.8 Hz, 1H), 8.08 (t, *J* = 7.7 Hz, 1H), 7.96 (d, *J* = 15.6 Hz, 1H), 7.85 – 7.76 (m, 2H), 7.73 (t, *J* = 7.9 Hz, 1H), 7.63 (t, *J* = 7.3 Hz, 1H), 7.56 (t, *J* = 7.6 Hz, 2H), 7.45 – 7.42 (m, 1H), 7.39 (d, *J* = 7.6 Hz, 1H), 7.34 (t, *J* = 7.8 Hz, 1H), 7.02 (dd, *J* = 8.1, 1.8 Hz, 1H), 3.78 (s, 3H). ^{13}C NMR (126 MHz, DMSO-d_6) δ 189.33, 159.77, 159.11, 158.02, 150.68, 144.23, 140.09, 138.33, 138.11, 136.18, 133.49, 130.41, 130.04, 129.09, 128.53 (2C), 128.32, 128.06, 126.56, 126.22, 123.94, 123.16, 122.60, 121.86, 121.67, 116.87, 114.56, 114.13, 113.60, 55.38. LC-MS (*m/z*): positive mode 458 $[M+H]^+$. Purity by HPLC-UV (254 nm)-ESI-MS: 99 %.

(E)-3-(3,4-dimethoxyphenyl)-1-(3-((2-(3,4-dimethoxyphenyl)quinazolin-4-yl) amino)phenyl)prop-2-en-1-one (24). The product was synthesized from 1-(3-((2-(3,4-dimethoxyphenyl)quinazolin-4-yl)amino)phenyl)ethanone (16) and 3,4-dimethoxybenzaldehyde to yield pale yellow solid (31 %). ^{1}H NMR (500 MHz, DMSO-d_6) δ 11.54 (s, 1H), 8.88 (d, *J* = 8.3 Hz, 1H), 8.69 (s, 1H), 8.42 – 8.33 (m, 1H), 8.17 – 8.11 (m, 3H), 8.08 – 8.04 (m, 2H), 7.84 (d, *J* = 15.5 Hz, 1H), 7.81 – 7.77 (m, 2H), 7.76 – 7.71 (m, 1H), 7.48 (d, *J* = 1.9 Hz, 1H), 7.36 (dd, *J* = 8.4, 1.9 Hz, 1H), 7.09 (d, *J* = 8.7 Hz, 1H), 7.00 (d, *J* = 8.4 Hz, 1H), 3.81 (s, 6H), 3.80 (s, 3H), 3.79 (s, 3H). ^{13}C NMR (126 MHz, DMSO-d_6) δ 188.70, 158.88, 156.82, 153.47, 151.61 (2C), 149.17, 148.88, 145.09, 138.42 (2C), 135.87 (2C), 129.20, 128.69, 127.84, 127.55, 126.18, 124.69, 124.35, 124.13, 119.62 (2C), 112.76, 111.71, 112.15, 111.75, 111.10, 55.94 (2C), 55.90, 55.79. One quaternary C atom is missing. LC-MS (*m/z*): positive mode 548 $[M+H]^+$. Purity by HPLC-UV (254 nm)-ESI-MS: 95 %.

(E)-1-(3-((2-(3,4-dimethoxyphenyl)quinazolin-4-yl)amino)phenyl)-3-(4-methoxy phenyl)prop-2-en-1-one (25). The product was synthesized from 1-(3-((2-(3,4-dimethoxyphenyl)quinazolin-4-yl)amino)phenyl)ethanone (**16**) and 4-methoxybenzaldehyde to yield yellow solid (18 %). ^{1}H NMR (500 MHz, DMSO-d_6) δ 10.03 (s, 1H), 8.78 (t, *J* = 1.9 Hz, 1H), 8.58 (d, *J* = 8.4 Hz, 1H), 8.30 – 8.25 (m, 1H), 8.10 (dd, *J* = 8.4, 2.0 Hz, 1H), 8.04 (d, *J* = 1.9 Hz, 1H), 7.99 (d, *J* = 7.8 Hz, 1H), 7.94 (d, *J* = 15.6 Hz, 1H), 7.86 (d, *J* = 3.6 Hz, 2H), 7.78 (d, *J* = 15.6 Hz, 1H), 7.66 (t, *J* = 7.9 Hz, 1H), 7.62 – 7.58 (m, 1H), 7.45 – 7.43 (m, 1H), 7.40 (d, *J* = 7.7 Hz, 1H), 7.34 (t, *J* = 7.9 Hz, 1H), 7.04 – 7.00 (m, 1H), 6.98 (d, *J* = 8.6 Hz, 1H), 3.81 (s, 3H), 3.78 (s, 3H), 3.76 (s, 3H). ^{13}C NMR (126 MHz, DMSO-d_6) δ 189.36, 159.79, 158.91, 157.83, 151.04, 150.81, 148.63, 144.28, 140.14, 138.09, 136.16, 133.41, 130.94, 130.05, 128.99, 128.12, 126.75, 125.75, 123.92, 123.14, 122.58, 121.93, 121.70, 121.28, 116.88, 113.89, 113.64, 111.46, 111.07, 55.62, 55.40, 55.36. LC-MS (*m/z*): positive mode 518 $[M+H]^+$. Purity by HPLC-UV (254 nm)-ESI-MS: 97 %.

(E)-1-(3-((2-(3,4-dimethoxyphenyl)quinazolin-4-yl)amino)phenyl)-3-(3-methoxyphenyl)prop-2-en-1-one (26). The product was synthesized from 1-(3-((2-(3,4-dimethoxyphenyl)quinazolin-4-yl)amino)phenyl)ethanone (**16**) and 3-methoxybenzaldehyde to yield pale yellow (20 %). ^{1}H NMR (500 MHz, DMSO-d_6) δ 11.57 (s, 1H), 8.86 (d, *J* = 8.1 Hz, 1H), 8.68 (s, 1H), 8.37 (d, *J* = 8.4 Hz, 1H), 8.15 (d, *J* = 7.9 Hz, 2H), 8.12 (dd, *J* = 8.5, 2.1 Hz, 1H), 8.07 (t, *J* = 7.8 Hz, 1H), 8.03 (d, *J* = 2.1 Hz, 1H), 7.95 (d, *J* = 15.6 Hz, 1H), 7.81 (d, *J* = 7.6 Hz, 1H), 7.78 (d, *J* = 15.6 Hz, 1H), 7.74 (t, *J* = 7.9 Hz, 1H), 7.43 (d, *J* = 2.0 Hz, 1H), 7.39 (d, *J* = 7.7 Hz, 1H), 7.34 (t, *J* = 7.8 Hz, 1H), 7.11 (d, *J* = 8.7 Hz, 1H), 7.02 (dd, *J* = 8.1, 1.8 Hz, 1H), 3.80 (s, 6H), 3.79 (s, 3H). ^{13}C NMR (126 MHz, DMSO) δ 188.90, 159.80, 158.91, 156.93, 156.91, 153.47, 148.91, 144.62, 138.12, 137.94, 136.08, 135.95, 130.07, 129.35, 128.91, 127.89, 127.82, 124.48, 124.35, 124.28, 123.51, 122.30, 121.78, 116.95, 113.72, 112.74, 112.01, 111.76, 55.98, 55.84, 55.46. One quaternary C atom is missing. LC-MS (*m/z*): positive mode 518 $[M+H]^+$. Purity by HPLC-UV (254 nm)-ESI-MS: 97 %.

(E)-3-(3,4-dimethoxyphenyl)-1-(4-(quinazolin-4-ylamino)phenyl)prop-2-en-1-one (27). Synthesized from 1-(4-(quinazolin-4-ylamino)phenyl)ethanone (**9**) and 3,4-dimethoxybenzaldehyde to obtain **27** as yellow solid (23 %). ^{1}H NMR (500 MHz, DMSO-d_6) δ 10.06 (s, 1H), 8.72 (s, *J* = 8.0 Hz, 1H), 8.62 (d, *J* = 8.3 Hz, 1H), 8.22 (d, *J* = 8.9 Hz, 2H), 8.18 (d, *J* = 8.7 Hz, 2H), 7.90 (t, *J* = 7.5 Hz, 1H), 7.88 – 7.82 (m, 2H), 7.73 – 7.66 (m, 2H), 7.54 (d, *J* = 1.8 Hz, 1H), 7.38 (dd, *J* = 8.3, 1.7 Hz, 1H), 7.03 (d, *J* = 8.3 Hz, 1H), 3.87 (s, 3H), 3.82 (s, 3H). ^{13}C NMR (126 MHz, DMSO-d_6) δ 187.61, 157.62, 154.34, 151.36, 150.01, 149.21, 143.96, 143.92, 133.45, 132.70, 129.51 (2C), 128.10, 127.82, 126.71, 123.93, 123.22, 121.03 (2C), 119.81, 115.50, 111.78, 110.94, 55.92, 55.76. LC-MS (*m/z*): positive mode 412 $[M+H]^+$. Purity by HPLC-UV (254 nm)-ESI-MS: 95 %.

(E)-3-(3-methoxyphenyl)-1-(4-(quinazolin-4-ylamino)phenyl)prop-2-en-1-one (28). Synthesized from 1-(4-(quinazolin-4-ylamino)phenyl)ethanone (**9**) and 3-methoxybenzaldehyde to obtain **28** as mustard solid (44 %). ^{1}H NMR (500 MHz, DMSO-d_6) δ 11.05 (s, 1H), 8.90 (s, 1H), 8.84 (d, *J* = 8.1 Hz, 1H), 8.27 (d, *J* = 8.8 Hz, 2H), 8.11 (d, *J* = 8.7 Hz, 2H), 8.06 – 8.02 (m, 1H), 7.98 (d, *J* = 15.6 Hz, 1H), 7.94 (d, *J* = 7.7 Hz, 1H), 7.84 – 7.79 (m, 1H), 7.73 (d, *J* = 15.6 Hz, 1H), 7.50 – 7.48 (m, 1H), 7.44 (d, *J* = 7.6 Hz, 1H), 7.37 (t, *J* = 7.9 Hz, 1H), 7.03 (dd, *J* = 8.1, 1.8 Hz, 1H), 3.84 (s, 3H). ^{13}C NMR (126 MHz, DMSO-d_6) δ 187.98, 159.83 (2C), 158.96, 152.63, 143.82, 142.62, 136.30, 135.19, 133.94, 130.08, 129.57 (2C), 127.94, 124.28, 123.72, 122.87, 122.45 (2C), 121.81, 116.81, 114.66, 113.54, 55.48. LC-MS (*m/z*): positive mode 382 $[M+H]^+$. Purity by HPLC-UV (254 nm)-ESI-MS: 97 %.

(E)-3-(3,4-dimethoxyphenyl)-1-(4-((6,7-dimethoxyquinazolin-4-yl)amino)phenyl) prop-2-en-1-one (29). Synthesized from 1-(4-((6,7-dimethoxyquinazolin-4-yl)amino)phenyl)ethanone (**11**) and 3,4-dimethoxybenzaldehyde to obtain **29** as mustard solid (29 %). ^{1}H NMR (500 MHz, DMSO-d_6) δ 11.54 (s, 1H), 8.89 (s, 1H), 8.42 (d, *J* = 2.0 Hz, 1H), 8.26 (d, *J* = 8.6 Hz, 2H), 8.04 – 8.00 (m, 2H), 7.86 (d, *J* = 15.5 Hz, 1H), 7.71 (d, *J* = 15.5

Hz, 1H), 7.54 (d, *J* = 1.9 Hz, 1H), 7.41 – 7.37 (m, 2H), 7.02 (d, *J* = 8.4 Hz, 1H), 4.04 (s, 3H), 3.99 (s, 3H), 3.87 (s, 3H), 3.82 (s, 3H). ^{13}C NMR (126 MHz, DMSO-d_6) δ 187.89, 158.10, 156.62, 151.49, 150.47, 149.20, 144.50, 141.58, 136.58, 135.00, 129.27 (2C), 127.69, 124.09, 124.00 (2C), 119.66, 111.76, 111.02, 107.92, 104.22, 100.27, 100.25, 57.21, 56.63, 55.94, 55.78. LC-MS (*m/z*): positive mode 472 $[M+H]^+$. Purity by HPLC-UV (254 nm)-ESI-MS: 96 %.

(E)-1-(4-((6,7-dimethoxyquinazolin-4-yl)amino)phenyl)-3-(3-methoxy phenyl) prop-2-en-1-one (30). Synthesized from 1-(4-((6,7-dimethoxyquinazolin-4-yl)amino)phenyl)ethanone (**11**) and 3-methoxybenzaldehyde to obtain **30** as yellow solid (44 %). ^{1}H NMR (500 MHz, DMSO-d_6) δ 9.73 (s, 1H), 8.58 (s, 1H), 8.23 (d, *J* = 8.8 Hz, 2H), 8.11 (d, *J* = 8.8 Hz, 2H), 7.97 (d, *J* = 15.6 Hz, 1H), 7.88 (s, 1H), 7.71 (d, *J* = 15.6 Hz, 1H), 7.48 (d, *J* = 2.1 Hz, 1H), 7.44 (d, *J* = 7.8 Hz, 1H), 7.37 (t, *J* = 7.9 Hz, 1H), 7.23 (s, 1H), 7.02 (dd, *J* = 7.9, 2.1 Hz, 1H), 3.99 (s, 3H), 3.94 (s, 3H), 3.84 (s, 3H). ^{13}C NMR (126 MHz, DMSO-d_6) δ 187.63, 159.82, 155.99, 154.70, 152.68, 149.31, 147.53, 144.62, 143.31, 136.40, 131.94, 130.04, 129.69 (2C), 122.52, 121.68, 120.76 (2C), 116.64, 113.50, 109.42, 107.40, 102.00, 56.43, 56.01, 55.45. LC-MS (*m/z*): positive mode 442 $[M+H]^+$. Purity by HPLC-UV (254 nm)-ESI-MS: 97 %.

(E)-3-(3,4-dimethoxyphenyl)-1-(4-((2-phenylquinazolin-4-yl)amino)phenyl)prop-2-en-1-one (31). Synthesized from 1-(4-((2-phenylquinazolin-4-yl)amino)phenyl)ethanone (**13**) and 3,4-dimethoxybenzaldehyde to obtain **31** as yellow solid (16 %). ^{1}H NMR (500 MHz, DMSO-d_6) δ 10.15 (s, 1H), 8.64 (d, *J* = 8.4 Hz, 1H), 8.50 (dd, 2H), 8.32 (d, *J* = 8.8 Hz, 2H), 8.26 (d, *J* = 8.8 Hz, 2H), 7.94 – 7.88 (m, 3H), 7.73 (d, *J* = 15.4 Hz, 1H), 7.69 – 7.64 (m, 1H), 7.59 – 7.50 (m, 4H), 7.41 (dd, *J* = 8.3, 1.8 Hz, 1H), 7.03 (d, *J* = 8.4 Hz, 1H), 3.88 (s, 3H), 3.82 (s, 3H). ^{13}C NMR (126 MHz, DMSO-d_6) δ 187.55, 159.10, 157.89, 151.37, 150.73, 149.22, 144.10, 144.02, 138.23, 133.70, 132.66, 130.61, 129.65 (2C), 128.71 (2C), 128.34, 128.11 (2C), 127.86, 126.41, 123.96, 123.31, 120.97 (2C), 119.76, 114.32, 111.78, 111.09,

55.97, 55.77. LC-MS (*m/z*): positive mode 488 $[M+H]^+$. Purity by HPLC-UV (254 nm)-ESI-MS: 96 %.

(E)-3-(3-methoxyphenyl)-1-(4-((2-phenylquinazolin-4-yl)amino)phenyl)prop-2-en-1-one (32). Synthesized 1-(4-((2-phenylquinazolin-4-yl)amino)phenyl)ethanone (**13**) and 3-methoxybenzaldehyde to obtain **32** as yellow solid (44 %). ^{1}H NMR (600 MHz, DMSO-d_6) δ 10.15 (s, 1H), 8.64 (d, *J* = 8.2 Hz, 1H), 8.52 – 8.49 (m, 2H), 8.33 (d, 2H), 8.28 (d, *J* = 8.8 Hz, 2H), 8.04 (d, *J* = 15.6 Hz, 1H), 7.93 – 7.90 (m, 2H), 7.74 (d, *J* = 15.5 Hz, 1H), 7.68 – 7.64 (m, 1H), 7.58 – 7.54 (m, 2H), 7.54 – 7.52 (m, 1H), 7.51 (d, *J* = 1.8 Hz, 1H), 7.46 (d, *J* = 7.6 Hz, 1H), 7.38 (t, *J* = 7.9 Hz, 1H), 7.03 (dd, *J* = 8.1, 2.0 Hz, 1H), 3.84 (s, 3H). ^{13}C NMR (151 MHz, DMSO-d_6) δ 187.63, 159.80, 159.06, 157.84, 150.78, 144.35, 143.45, 138.23, 136.38, 133.67, 132.25, 130.57, 130.02, 129.80 (2C), 128.68 (2C), 128.37, 128.07 (2C), 126.39, 123.28, 122.45, 121.75, 120.90 (2C), 116.63, 114.31, 113.57, 55.45. LC-MS (*m/z*): positive mode 458 $[M+H]^+$. Purity by HPLC-UV (254 nm)-ESI-MS: 97 %.

(E)-3-(4-methoxyphenyl)-1-(4-((2-phenylquinazolin-4-yl)amino)phenyl)prop-2-en-1-one (33). Synthesized 1-(4-((2-phenylquinazolin-4-yl)amino)phenyl)ethanone (**13**) and 4-methoxybenzaldehyde to obtain **33** as yellow solid (41 %). ^{1}H NMR (500 MHz, DMSO-d_6) δ 10.13 (s, 1H), 8.64 (d, *J* = 8.4 Hz, 1H), 8.53 – 8.48 (m, 2H), 8.32 – 8.28 (m, 2H), 8.28 – 8.25 (m, 2H), 7.92 – 7.91 (m, 2H), 7.90 – 7.85 (m, 3H), 7.74 (d, *J* = 15.5 Hz, 1H), 7.68 – 7.64 (m, 1H), 7.58 – 7.49 (m, 3H), 7.06 – 7.03 (m, 2H), 3.83 (s, 3H). ^{13}C NMR (126 MHz, DMSO-d_6) δ 187.53, 161.41, 159.08, 157.85, 150.78, 144.09, 143.41, 138.26, 133.66, 132.60, 130.83 (2C), 130.57, 129.60 (2C), 128.68 (2C), 128.38, 128.08 (2C), 127.64, 126.38, 123.27, 120.93 (2C), 119.71, 114.53 (2C), 114.31, 55.51. LC-MS (*m/z*): positive mode 458 $[M+H]^+$. Purity by HPLC-UV (254 nm)-ESI-MS: 99 %.

(E)-3-phenyl-1-(4-((2-phenylquinazolin-4-yl)amino)phenyl)prop-2-en-1-one (34). Synthesized 1-(4-((2-phenylquinazolin-4-yl)amino)phenyl)ethanone (**13**) and benzaldehyde to obtain **34** as yellow solid (43 %). ^{1}H NMR (500 MHz, DMSO-d_6) δ 11.51 (s, 1H), 8.96 (d, *J* =

8.3 Hz, 1H), 8.45 (d, *J* = 7.0 Hz, 2H), 8.36 – 8.29 (m, 3H), 8.18 (d, *J* = 8.7 Hz, 2H), 8.11 – 8.06 (m, 1H), 8.02 (d, *J* = 15.6 Hz, 1H), 7.91 (dd, *J* = 6.6, 2.8 Hz, 2H), 7.82 (t, *J* = 7.7 Hz, 1H), 7.78 (d, *J* = 15.6 Hz, 1H), 7.71 – 7.62 (m, 3H), 7.51 – 7.44 (m, 3H). ^{13}C NMR (126 MHz, DMSO-d_6) δ 187.99, 159.01, 157.82, 143.95, 142.16, 135.77, 134.88, 134.37, 132.94 (2C), 130.75, 129.56 (2C), 129.21 (2C), 129.13 (2C), 129.05, 129.04, 128.03 (2C), 124.60, 123.41 (2C), 122.16 (2C), 113.37. One signal for –C is missing. LC-MS (*m/z*): positive mode 428 $[M+H]^+$. Purity by HPLC-UV (254 nm)-ESI-MS: 96 %.

(E)-3-(3,4-dimethoxyphenyl)-1-(4-((2-(3,4-dimethoxyphenyl)quinazolin-4-yl) amino)phenyl)prop-2-en-1-one (35). Synthesized from 1-(4-((2-(3,4-dimethoxyphenyl)quinazolin-4-yl)amino)phenyl)ethanone (**15**) and 3,4-dimethoxybenzaldehyde to obtain **35** as yellow solid (28 %). ^{1}H NMR (500 MHz, DMSO-d_6) δ 10.10 (s, 1H), 8.59 (d, *J* = 8.4 Hz, 1H), 8.30 – 8.25 (m, 4H), 8.11 – 8.08 (m, 2H), 7.90 – 7.86 (m, 3H), 7.72 (d, *J* = 15.4 Hz, 1H), 7.64 – 7.59 (m, 1H), 7.56 (d, *J* = 2.0 Hz, 1H), 7.40 (dd, *J* = 8.4, 1.9 Hz, 1H), 7.13 (d, *J* = 9.0 Hz, 1H), 7.03 (d, *J* = 8.4 Hz, 1H), 3.90 (s, 3H), 3.88 (s, 3H), 3.84 (s, 3H), 3.82 (s, 3H). ^{13}C NMR (126 MHz, DMSO-d_6) δ 187.59, 158.87, 157.61, 151.37, 151.17, 150.94, 149.21, 148.71, 144.18, 143.97, 133.57, 132.63, 130.85, 129.49 (2C), 128.19, 127.84, 125.90, 123.91, 123.24, 121.35, 121.05 (2C), 119.80, 114.05, 111.79, 111.64, 111.13, 111.05, 55.94, 55.77, 55.73, 55.47. LC-MS (*m/z*): positive mode 548 $[M+H]^+$. Purity by HPLC-UV (254 nm)-ESI-MS: 98 %.

(E)-1-(4-((2-(3,4-dimethoxyphenyl)quinazolin-4-yl)amino)phenyl)-3-(3-methoxy phenyl)prop-2-en-1-one (36). Synthesized from 1-(4-((2-(3,4-dimethoxyphenyl)quinazolin-4-yl)amino)phenyl)ethanone (**15**) and 3-methoxybenzaldehyde to obtain **36** as ochre solid (39 %). ^{1}H NMR (500 MHz, DMSO-d_6) δ 11.52 (s, 1H), 8.87 (d, *J* = 8.3 Hz, 1H), 8.42 (d, *J* = 7.5 Hz, 1H), 8.33 (d, *J* = 8.8 Hz, 2H), 8.15 – 8.11 (m, 4H), 8.06 (t, *J* = 8.1 Hz, 1H), 7.99 (d, *J* = 15.6 Hz, 1H), 7.79 (t, *J* = 7.6 Hz, 1H), 7.74 (d, *J* = 15.6 Hz, 1H), 7.51 – 7.48 (m, 1H), 7.45 (d, *J* = 7.6 Hz, 1H), 7.38 (t, *J* = 7.9 Hz, 1H), 7.22 (d, *J* = 8.5 Hz, 1H), 7.07 – 7.02 (m, 1H), 3.89

(s, 3H), 3.87 (s, 3H), 3.84 (s, 3H). ^{13}C NMR (126 MHz, DMSO-d_6) δ 188.06, 159.84 (2C), 158.75, 156.87, 153.46, 148.92, 144.04, 141.91, 136.26 (2C), 135.92, 134.67, 130.10, 129.45 (2C), 127.84, 124.56, 123.86, 123.68, 122.37 (2C), 121.81, 116.81 (2C), 113.67, 112.93, 112.14, 111.90, 56.04, 55.99, 55.49. LC-MS (*m/z*): positive mode 518 $[M+H]^+$. Purity by HPLC-UV (254 nm)-ESI-MS: 100 %.

(E)-1-(4-((2-(3,4-dimethoxyphenyl)quinazolin-4-yl)amino)phenyl)-3-(4-methoxyphenyl)prop-2-en-1-one (37). Synthesized from 1-(4-((2-(3,4-dimethoxyphenyl)quinazolin-4-yl)amino)phenyl)ethanone (**15**) and 4-methoxybenzaldehyde to obtain **37** as ochre solid (37 %). ^{1}H NMR (500 MHz, DMSO-d_6) δ 11.25 (s, 1H), 8.80 (d, *J* = 8.2 Hz, 1H), 8.31 (d, *J* = 8.7 Hz, 2H), 8.15 – 8.10 (m, 4H), 8.05 (t, *J* = 7.6 Hz, 1H), 7.89 – 7.83 (m, 4H), 7.80 – 7.77 (m, 1H), 7.75 (d, *J* = 15.5 Hz, 1H), 7.22 (d, *J* = 8.9 Hz, 1H), 7.04 (d, *J* = 8.8 Hz, 2H), 3.90 (s, 3H), 3.88 (s, 3H), 3.83 (s, 3H). ^{13}C NMR (126 MHz, DMSO-d_6) δ 187.87, 161.56 (2C), 158.62, 156.93, 153.31, 148.88, 143.99, 141.82, 135.73, 134.84, 131.04, 130.93 (2C), 130.38, 129.25 (2C), 127.70, 127.51 (2C), 124.50, 123.68, 123.56, 119.58, 114.59 (2C), 112.96, 112.07, 111.85, 56.01, 55.96, 55.55.

LC-MS (*m/z*): positive mode 518 $[M+H]^+$. Purity by HPLC-UV (254 nm)-ESI-MS: 99 %.

(E)-1-(4-((2-(3,4-dimethoxyphenyl)quinazolin-4-yl)amino)phenyl)-3-phenylprop-2-en-1-one (38). Synthesized from 1-(4-((2-(3,4-dimethoxyphenyl)quinazolin-4-yl)amino)phenyl)ethanone (**15**) and benzaldehyde to obtain 38 as yellow solid (19 %). ^{1}H NMR (500 MHz, DMSO-d_6) δ 11.39 (s, 1H), 8.83 (d, *J* = 8.2 Hz, 1H), 8.34 (d, *J* = 8.7 Hz, 3H), 8.16 – 8.11 (m, 4H), 8.07 (t, *J* = 7.8 Hz, 1H), 8.00 (d, *J* = 15.6 Hz, 1H), 7.93 – 7.88 (m, 2H), 7.79 (dd, *J* = 15.4, 8.0 Hz, 2H), 7.51 – 7.45 (m, 3H), 7.23 (d, *J* = 9.1 Hz, 1H), 3.90 (s, 3H), 3.88 (s, 3H). ^{13}C NMR (126 MHz, DMSO-d_6) δ 188.14, 158.75, 156.74, 153.59, 148.94 (2C), 144.13, 141.80, 141.39, 136.05, 134.88 (2C), 134.79, 130.87, 129.42 (2C), 129.16 (2C), 129.08 (2C), 127.97, 124.64, 123.99 (2C), 123.79, 122.14, 112.85, 112.14, 111.89, 56.08,

56.02. LC-MS (*m/z*): positive mode 488 $[M+H]^+$. Purity by HPLC-UV (254 nm)-ESI-MS: 95 %.

Biological Investigation. Materials. Ko143 and cyclosporine A were purchased from Tocris Bioscience (Bristol, United Kingdom). Pheophorbide A was supplied by Fontier Scientific Inc. (Logan, UT, USA) and calcein AM was delivered by Merck KGaA (Darmstadt, Germany). All cell culture material was provided by Sarstedt (Newton, USA) and all other chemicals were purchased from Sigma-Aldrich Chemicals (Taufkirchen, Germany) unless otherwise stated.

Cell culture. The cell lines MDCK II wild type and the transfected cell line MDCK II BCRP were a generous gift of Dr. A. Schinkel (The Netherlands Cancer Institute, Amsterdam, The Netherlands). The MDCK II BCRP cell line stably expressing the breast cancer resistance protein (BCRP, ABCG2) was generated by transfection of the canine kidney epithelial cell line MDCK II with the human wild-type cDNA C-terminally linked to the cDNA of the green fluorescent protein (GFP). These cells were grown in Dulbecco's modified eagle medium (DMEM) supplemented with 10 % fetal bovine serum (FBS), 50 µg/µl streptomycin, 50 units/ml penicillin G and 2 mM L-glutamine. The breast cancer cell line MCF-7 MX and the parental cell line MCF-7 were kindly provided by Dr. E. Schneider, Wadsworth Center, Albany, NY, USA. The cells were cultured in RPMI-1640 medium supplemented with 20 % FBS, 50 µl/ml streptomycin, 50 units/ml penicillin G and 2 mM L-glutamine. To maintain ABCG2 overexpression, mitoxantrone was added in a final concentration of 0.1 µM every 10 passages. The small cell lung cancer cell line H69AR overexpressing the multidrug resistance associated protein 1 (MRP1, ABCC1) was purchased from ATCC (CRL-11351) and grown in the same medium as described for MCF-7 cells. Human ovarian carcinoma cell line A2780 and the corresponding P-glycoprotein (P-gp, ABCB1) overexpressing doxorubicin resistant A2780adr cell line were purchased from ECACC (Nos. 93112519 and 93112520). The cell

lines were cultured in RPMI-1640 medium supplemented with 10 % FBS, 50 µl/ml streptomycin, 50 units/ml penicillin G and 2 mM L-glutamine. To maintain doxorubicin resistance the cells were kept under doxorubicin in a concentration of 1 µM (for one passage) every 10 passages. All cells were grown as adherent monolayer cultures under humidified atmosphere with 5 % CO_2 and a temperature of 37 °C. After reaching confluence of 80-90 %, subculturing was performed with 0.05 % trypsin and 0.02 % EDTA.

Pheophorbide A assay. The pheophorbide A accumulation assay was performed as described earlier using MDCK II wild type and MDCK II BCRP cells.[26,48,17,27] When reaching a confluence of 80-90 % in T75- or T175-flasks the cells were harvested by gentle trypsination (0.05 % trypsin/0.02 % EDTA) with subsequent centrifugation (266 g, 4 °C, 4 min). The obtained cell pellet was dispersed in fresh culture medium and the cell density was determined using a CASY 1 Modell TT cell counter device (Schaerfe System GmbH, Reutlingen, Germany). The required amount of cells was washed twice with KHB and seeded into U-shaped clear 96 well plates (Greiner, Frickenhausen, Germany) at a density of approximately 45,000 cells per well in a volume of 160 µl. The various test compounds prepared in different concentrations were added in a volume 20 µl per well. After a preincubation period of 20 min under standard cultivation conditions (5 % CO_2, 37 °C), 20 µl of a 5 µM pheophorbide A solution (protected from light) was added to each well. To achieve steady state conditions the completely prepared 96 well plate was kept under 5 % CO_2 and 37 °C for 120 min. Before starting measurement the cells were resuspended to get a homogeneous suspension and to remove adherent cells from the bottom. Fluorescence was measured by flow cytometry (FACScalibur, Becton Dickinson Biosciences, Heidelberg, Germany). An argon laser with an excitation wavelength of 488 nm excited pheophorbide A which could be detected at a wavelength range over 670 nm in the FL_3 channel. To quantify and assure ABCG2 overexpression, GFP was detected in the FL_1 channel at a wavelength of 530/15 nm. Concentration response curves were generated by nonlinear regression using the

4-parameter logistic equation (GraphPad Prism 5.03 software, San Diego, CA, USA). Experiments were carried out in duplicate.

Enzyme kinetic experiments were conducted to analyse the type of interaction of compound **35** with pheophorbide A. Various pheophorbide A concentrations (0.2, 0.4, 0.5, 1.0, 1.5 and 2.0 µM) as well as of compound **35** were investigated. For data analysis Lineweaver-Burk linearization technique was applied and the type of interaction was determined according to changes in the K_M and V_{max} values.

Calcein AM assay. The calcein AM assay was used to determine the ABCB1 and ABCC1 inhibition in order to confirm the selectivity of the compounds toward ABCG2. [52,53,54] The ABCB1 overexpressing cell line A2780adr and the ABCC1 overexpressing cell line H69AR were used. After reaching a confluence of 80-90 % the cells were harvested by trypsination and subsequently centrifuged at 266 g and 4 °C for 4 min and prepared as described above. The cells were seeded into clear flat bottom 96 well plates (Greiner, Frickenhausen, Germany) at a density of approximately 30,000 cells in a volume of 90 µl per well, adding of 10 µl of the test compounds in different concentrations. After an incubation time of 30 min, 33 µl of a 1.25 µM calcein AM solution (protected from light) was added to each well. Fluorescence was measured immediately in constant time intervals of 60 s up to 3600 s at an excitation wavelength of 485 nm and an emission wavelength of 520 nm utilizing a 37 °C tempered BMG POLARstar microplate reader (BMG LABTECH, Offenburg, Germany). The fluorescence increase obtained in the presence of calcein correlates with the inhibition level of ABCB1 and ABCC1 and was used to generate dose-response curves by nonlinear regression using the four parameter logistic equation with variable slope. Normalization was performed using cyclosporine A as standard inhibitor for ABCB1 and ABCC1.

ATPase activity measurements. *Spodoptera Frugiperda* (Sf9) ovarian cells were grown in protein-free insect medium (Spodopan, PAN-Biotech GmbH, Aidenbach, Germany)

supplemented with 50 µg/ml streptomycin, 50 units/ml penicillin G and 0.125 µg/ml Fungizone® antimycotic as adherent monolayer culture. The recombinant baculovirus, carrying the human wild-type ABCG2 cDNA, was a generous gift from Dr. Csilla Özvegy-Laczka (Research Centre for Natural Sciences, Hungarian Academy of Sciences, Budapest, Hungary). Cell infection for membrane preparation was performed by seeding 3 x 10^7 cells in a T175 culture flask. Three days after virus transfection, the Sf9 cells were harvested and their membranes were isolated including a cholesterol-loading step as described earlier.[7,55,56] The amount of the membrane protein was determined by a bicinchoninic acid assay (BCA assay). Vanadate-sensitive ATPase activity was measured by a colorimetric reaction between ascorbic acid and free inorganic phosphate from ATP hydrolysis. The reaction mixture contained 40 mM 3-(N-morpholino)propanesulfonic acid-Tris (pH 7.0), 50 mM KCl, 2 mM dithiothreitol, 500 µM EGTA-Tris (pH 7.0), 5 mM sodium azide, 1 mM oubain and 10 µg membrane protein (1 mg/ml). The ATPase reaction was started by addition of 3.3 mM MgATP and continued for 20 min at 37 °C. The basal activity was determined in the presence of 1 mM sodium othovanadate. ATPase activation was performed with 1 µM quercetin and ATPase inhibition with 1 µM Ko143. The reaction was stopped by addition of 100 µl 5 % SDS (sodium dodecyl sulfate). The colorimetric detection was performed by addition of 300 µl P_i-reagent (2.5 M H_2SO_4, 1 % ammonium molybdate, 0.014 % antimony potassium tartrate), 750 µl 20 % acetic acid and 150 µl 1 % freshly prepared ascorbic acid. After an incubation time of 20 min the optical density was measured at room temperature at a wavelength of 880 nm. K_2HPO_4 was used as standard for calculating the amount of phosphate from the absorbance values.

Confocal laser scanning microscopy. Confocal laser scanning microscopy was used to get an optical evidence of accumulation of compound **27** and to investigate the transport by ABCG2. For each probe 1 x 10^5 MCF-7 MX or parental MCF-7 cells were seeded into low µ-dish (ibidi GmbH, München, Germany) for 48 hours. After reaching a confluence of 50-60 %

the tested compound was added to the cells in a dilution factor of 10. Plates were further incubated for 2 h and restocked with 900 µl KHB after removing the supernatants. The fluorescence of cells was measured immediately using an excitation wavelength of 405 nm and an emission wavelength in a range from 425 to 475 nm with a Nikon A1 R microscope (Nikon, Düsseldorf, Germany) tempered at 37 °C. For visualizing accumulated compound the Nikon NIS Elements software was used (Nikon, Düsseldorf, Germany).

Transport studies by fluorescence spectroscopy. Fluorescence spectroscopy was used to investigate the accumulation of fluorescent compound **27** in ABCG2 overexpressing MCF-7 MX and parental MCF-7 cells. For the sample preparation the cells were prepared as described in the accumulation assay above. For each probe 1 x 10^6 cells per 4.5 ml in KHB were transferred in a 15 ml Falcon and 500 µl of compound **27** was added. After incubation for the desired period and a washing step with KHB the fluorescence inside the cell was determined using a LS 55 Fluorescence Spectrometer (PerkinElmer, Waltham, MA, USA).

MTT assay. The intrinsic cytotoxicity of tested compounds was ascertained in the MTT cytotoxicity assay by using MDCK II wild type and MDCK II BCRP cells.[25,26,**Error! Bookmark not defined.**] Compounds potent for ABCB1 were also screened for their cytotoxicity in ABCB1 overexpressing A2780adr and parental A2780 cells. The cells were harvested and seeded into 96-well tissue culture plates (Sarstedt, Newton, USA) with a density of 3 x 10^3 cells per well (8 x 10^3 cells for ABCB1 screening) in 180 µl and allowed to attach for 6 hours at 37 °C under 5 % CO_2. 20 µl of the tested compounds were added to each well. 10 % (v/v) DMSO and pure growth medium were used as positive and negative control. The interspaces of the plates were filled with PBS buffer to lower evaporation of solvent during the incubation time of 72 h. To detect the vitality of the cells 40 µl of a 5 mg/ml solution of the MTT reagent (3-(4,5-dimethylthiazol-2-yl)-2,5-diphenyltetrazolium bromide) was added to each well. After an incubation time of 1 h the reaction was stopped by removal of the supernatant and restocking with 100 µl DMSO per well. The absorbance was measured at 570 nm and background

correction at 690 nm using a Multiscan Ex microplate photometer (Thermo Fisher Scientific, Waltham, MA, USA). The data obtained were normalized and GI_{50} values were calculated by nonlinear regression analysis, assuming a sigmoidal concentration response curve with variable Hill slope.

To determine the multidrug resistance reversal ability of synthesized compounds similar experiments were performed. The effect on the cytotoxicity of SN-38 was measured in presence of selected compounds at a final concentration of 0.01 µM and 0.1 µM.

Pharmacophore search.

Compound 35 being the most active compound was overlaid on the pharmacophore model previously reported by Matsson et. al.[50].

All calculations were carried out using Molecular Operating Environment (MOE).[57] The 3D structure was generated using the Builder plugin of MOE and subsequently energy minimized using the MMFF94x force field. Pharmacophore features were generated using the Pharmacophore Editor. Conformational analysis was performed using systematic method and the MMFF94x force field. All conformations were subsequently refined with a semi empirical QM optimization using MOPAC 7 and PM3 as basis set. For other settings default options were used.

Low-energy conformations were mapped on the generated pharmacophore. Matched conformations were analyzed regarding their RMSD fit and their potential energy. Conformations with a low energy and a RMSD value < 0.3 were selected as good matches.

AUTHOR INFORMATION

Corresponding Author

*Phone: +49 228 735213. Fax: +49 228 737929. E-mail: mwiese@uni-bonn.de

Author Contributions

The manuscript was written by contributions of all authors. All authors have given approval to the final version of the manuscript. ‡These authors contributed equally.

Notes

The authors declare no competing financial interest.

Acknowledgement

The authors thank to Dr. A. H. Schinkel (The Netherlands Cancer Institute, Amsterdam, The Netherlands) for the MDCK II wild-type and MDCK II BCRP cell lines. We thank Dr. Csilla Özvegy-Laczka, Research Centre for Natural Sciences, Hungarian Academy of Sciences, Budapest, for kindly providing the recombinant ABCG2-baculovirus and for the instructions regarding the ATPase assay. Furthermore we thank our group members Anna Spindler and Michael Krapf for the evaluation of the MTT cytotoxicity data of Ko143.

ABBREVIATIONS USED

ABC, ATP-binding cassette; BCRP, breast cancer resistance protein;

References

[1] M.M. Gottesmann, Mechanisms of cancer drug resistance, Annu. Rev. Med. 53 (2002) 615-627.

[2] G. Szakács, J.K. Paterson, J.A. Ludwig, C. Booth-Genthe, M.M. Gottesmann, Targeting multidrug resistance in cancer, Nat. Rev. Drug Discov. 5 (2006) 5, 219-234.

[3] C.F. Higgins, ABC transporters: from microorganisms to man, Annu. Rev. Cell Biol. 8 (1992) 67-113.

[4] L.A. Doyle, W. Yang, L.V. Abruzzo, T. Krogmann, Y. Gao, A.K. Rishi, D.D. Ross, A multidrug resistance transporter from human MCF-7 breast cancer cells, Proc. Natl. Acad. Sci. U S A 95 (1998) 15665-15670.

[5] L.A. Doyle, D.D. Ross, Multidrug resistance mediated by the breast cancer resistance protein BCRP (ABCG2), Oncogene 22 (2003) 7340–7358.

[6] H. Wang, E.W. Lee, X. Cai, Z. Ni, L. Zhou, Q. Mao, Membrane topology of the human breast cancer resistance protein (BCRP/ABCG2) determined by epitope insertion and immunofluorescence, Biochemistry 47 (2008) 13778-13787.

[7] C. Özvegy, T. Litman, G. Szakaćs, Z. Nagy, S. Bates, A. Vaŕadi, B. Sarkadi, Functional characterization of the human multidrug transporter, ABCG2, expressed in insect cells, Biochem. Biophys. Res. Commun. 285 (2001) 111-117.

[8] K. Wong, S.J. Briddon, N.D. Holliday, I.D. Kerr, Plasma membrane dynamics and tetrameric organisation of ABCG2 transporters in mammalian cells revealed by single particle imaging techniques, Biochim. Biophys. Acta 1863 (2016), 19-29.

[9] K. Natarajan, Y. Xie, M.R. Baer, D.D. Ross, Role of Breast cancer resistance protein (BCRP/ABCG2) in cancer drug resistance, Biochem. Pharmacol. 83 (2012) 1084-1103.

[10] T. Litman, M. Brangi, E. Hudson, P. Fetsch, P. Abati, D.D. Ross, K. Miyake, J.H. Resau, S. Bates, The multidrug-resistant phenotype associated with overexpression of the new ABC half-transporter, MXR (ABCG2), J. Cell Sci.113 (2000) 2011-2021.

[11] J.W. Jonker, M. Buitelaar, E. Wagenaar, M.A. Van Der Valk, G.L. Scheffer, R.J. Scheper, T. Plosch, F. Kuipers, R.P. Elferink, H. Rosing, J.H. Beijnen, A.H. Schinkel, The breast cancer resistance protein protects against a major chlorophyll-derived dietary phototoxin and protoporphyria, Proc. Natl. Acad. Sci. U S A 99 (2002) 15649-15654.

[12] S. Rabindran, D. Ross, L. Doyle, W. Yang, L. Greenberger, Fumitremorgin C reverses multidrug resistance in cells transfected with the breast cancer resistance protein, Cancer Res. 60 (2000) 47-50.

[13] S. Rabindran, H. He, M. Singh, E. Brown, K. Collins, T. Annable, L. Greenberger, Reversal of a novel multidrug resistance mechanism in human colon carcinoma cells by Fumitremorgin C, Cancer Res. 58 (1998) 5850-5858.

[14] M. Nishiyama, T. Kuga, Central effects of the neurotropic mycotoxin fumitremorgin A in the rabbit (1): effects on the spinal cord, Jpn. J. Pharmacol. 50 (1989) 167 –173.

[15] A. Van Loevezijn, J.D. Allen, A.H. Schinkel, G.-J. Koomena, Inhibition of BCRP-mediated drug efflux by fumitremorgin-type indolyl diketopiperazines, Bioorg. Med. Chem. Lett. 11 (2001) 29-32.

[16] A. Pick, H. Müller, M. Wiese, Structure–activity relationships of new inhibitors of breast cancer resistance protein (ABCG2), Bioorg. Med. Chem. 16 (2008) 8224-8236.

[17] A. Pick, W. Klinkhammer, M. Wiese, Specific inhibitors of the Breast Cancer Resistance Protein (BCRP), ChemMedChem 5 (2010) 1498-1505.

[18] F. Marighetti, K. Steggemann, M. Hanl, M. Wiese, Synthesis and Quantitative Structure-Activity Relationships of selective BCRP Inhibitors, ChemMedChem 8 (2013) 125-135.

[19] F. Marighetti, K. Steggemann, M. Karbaum, M. Wiese, Scaffold identification of a new class of potent and selective BCRP-inhibitors, ChemMedChem 10 (2015) 742-751.

[20] S.C. Köhler, M. Wiese, HM30181 Derivatives as Novel Potent and Selective Inhibitors of the Breast Cancer Resistance Protein (BCRP/ABCG2), J. Med. Chem. 58 (2015) 3910-3921.

[21] K. Juvale, K. Stefan, M. Wiese, Synthesis and biological evaluation of flavones and benzoflavones as inhibitors of BCRP/ABCG2. Eur. J. Med. Chem. 67 (2013) 115-126.

[22] J. Gallus, K. Juvale, M. Wiese, Characterization of 3-Methoxy Flavones for their Interaction with ABCG2 as suggested by ATPase Activity. Biochim. Biophys. Acta 1838 (2014) 2929-2938.

[23] A. Pick, H. Müller, R. Mayer, B. Haenisch, I.K. Pajeva, M. Weigt, H. Bönisch, C.E. Müller, M. Wiese, Structure–activity relationships of flavonoids as inhibitors of breast cancer resistance protein (BCRP), Bioorg. Med. Chem. 19 (2011) 2090-2102.

[24] M.S. Singh, K. Juvale, M. Wiese, A. Lamprecht, Evaluation of dual P-gp-BCRP inhibitors as nanoparticle formulation, Eur. J. Pharm. Sci. 77 (2015) 1-8.

[25] K. Juvale, V.F. Pape, M. Wiese, Investigations of chalcones and benzochalcones as inhibitors of breast cancer resistance protein, Bioorg. Med. Chem. 20 (2012) 346-355.

[26] K. Juvale, J. Gallus, M. Wiese, Investigation of quianzolines as inhibitors of breast cancer resistance protein (ABCG2). Bioorg. Med. Chem. 21 (2013) 7858-7873.

[27] A. Pick, M. Wiese, Tyrosine kinase inhibitors influence ABCG2 expression in EGFR-positive MDCK BCRP cells via the PI3K/Akt signaling pathway, ChemMedChem 7 (2012) 650-662.

[28] K. Juvale, M. Wiese, 4-Substituted-2-phenylquinazolines as inhibitors of BCRP, Bioorg. Med. Chem. Lett. 22 (2012) 6766-6769.

[29] E. Winter, G.J. Gozzi, L. Domeneghini, C.-Delatorre, N. Daflon-Yunes, R. Terreux, C. Gauthier, A. Mascarello, P.C. Leal, S. M. Cadena, R.A. Yunes, R.J. Nunes, T.B. Creczynski-Pasa, A. Di Pietro, Quinoxaline-substituted chalcones as new inhibitors of breast cancer resistance protein ABCG2: polyspecificity at B-ring position. Drug Des. Devel. Ther. 8 (2014) 609-619.

[30] M.M. Pires, D. Emmert, C.A. Hrycyna,. Inhibition of P-Glykoprotein-Mediated Paclitaxel Resistance by Reversibly Linked Quinine Homodimers, Mol. Pharmacol. 75 (2009) 92-100.

[31] K.-F. Chan, Y. Zhao, B.A. Burkett, I.L.K. Wong, L.M.C. Chow, T.H. Chan, Flavonoid Dimers as Bivalent Modulators for P-Glycoprotein-Based Multidrug Resistance: Synthetic Apigenin Homodimers Linked with Defined-Length Poly(ethylene glycol) Spacers Increase Drug Retention and Enhance Chemosensitivity in Resistant Cancer cells. J. Med. Chem. 49 (2006) 6742-6759.

[32] K.-F. Chan, I.L.K Wong, J.W.Y. Kan, C.S.W. Yan, L.M.C. Chow, T.H. Chan, Amine Linked Flavonoid Dimers as Modulators for P-Glycoprotein-Based Multidrug Resistance: Structure-Activity Relationship and Mechanism of Modulation. J. Med. Chem. 55 (2012) 1999-2014.

[33] H.A. Namanja, E. Emmert, M.M. Pires, C.A. Hrycyna, J. Chmielewski, Inhibition of Human P-glycoprotein Transport and Substrate Binding Using a Galantamine Dimer. Biochem. Biophys. Res. Commun. 388 (2009) 672-676.

[34] R. Badhan, J. Penny, In silico modelling of the interaction of flavonoids with human P-glycoprotein nucleotide-binding domain, Eur. J. Med. Chem. 41 (2006) 285-295.

[35] J. Boccard, F. Bajot, A. Di Pietro, S. Rudaz, A. Boumendjel, E. Nicolle, P.-A. Carrupt, A 3D solvation energy model to quantify the affinity of flavonoid derivatives toward P-glycoprotein, Eur. J. Pharmacol. Sci. 36 (2009) 254-264.

[36] G. Kothandan, C. G. Gadhe, T. Madhavan, C. H. Choi, S. J. Cho, Docking and 3D-QSAR (quantitative structure activity relationship) studies of flavones, the potent inhibitors of p-glycoprotein targeting the nucleotide binding domain, Eur. J. Med. Chem. 46 (2011) 4078-4088.

[37] M. E. Morris, S. Zhang, Flavonoid–drug interactions: Effects of flavonoids on ABC transporters, Life Sci. 78 (2006) 2116-2130.

[38] F. Bois, C. Beney, A. Boumendjel, A.M. Mariotte, G. Conseil, A. Di Pietro, Halogenated chalcones with high-affinity binding to P-glycoprotein: potential modulators of multidrug resistance, J. Med. Chem. 41 (1998) 4161–4164.

[39] F. Bois, A. Boumendjel, A.M. Mariotte, G. Conseil, A. Di Petro, Synthesis and biological activity of 4-alkoxy chalcones: potential hydrophobic modulators of P-glycoprotein-mediated multidrug resistance, Bioorg. Med. Chem. 7 (1999) 2691–2695.

[40] E.B. Yang, K. Zhang, L.Y. Cheng, P. Mack, Butein, a specific protein tyrosine kinase inhibitor. Biochem. Biophys. Res. Commun. 245 (1998) 435–438.

[41] E.B. Yang, Y.J. Guo, K. Zhang, Y.Z. Chen, P. Mack, Inhibition of epidermal growth factor receptor tyrosine kinase by chalcone derivatives, Biochim. Biophys. Acta. 1550 (2001) 144–152.

[42] S. Rancon, A. Chaboud, N. Darbour, G. Comte, C. Bayet, P.N. Simon, J. Raynaud, A. Di Pietro, P. Cabalion, D. Barron, Natural and synthetic benzophenones: interaction with the cytosolic binding domain of P-glycoprotein, Phytochemistry 57 (2001) 553-557.

[43] A. Levitzki A. Protein tyrosine kinase inhibitors as novel therapeutic agents. Pharmacol. Ther. 82 (1999) 231–239.

[44] T. Hou, L. Zhu, L. Chen, X. Ku, Mapping the Binding Site of a Large Set of Quinazoline Type EGF-R Inhibitors Using Molecular Field Analyses and Molecular Docking Studies, J. Chem. Inf. Comput. Sci. 43 (2003) 273–287.

[45] D. Brehmer, Z. Greff, K. Godl, S. Blencke, A. Kurtenbach, et al., Cellular Targets of Gefitinib, Cancer Res. 65 (2005) 379-382.

[46] S.S. Suneet, Z.-S. Chen, S.V. Ambudkar, Tyrosine kinase inhibitors as modulators of ABC transporter-mediated drug resistance, Drug Resist. Updat. 15 (2012) 70-80.

[47] H. Saito, H. Hirano, H. Nakagawa, et al., A New Strategy of High-Speed Screening and Quantitative Structure-Activity Relationship Analysis to Evaluate Human ATP-Binding Cassette Transporter ABCG2-Drug Interactions, J. Pharmacol. Exp. Ther. 317 (2006) 1114-1124.

[48] A. Pick, H. Müller, M. Wiese, Novel lead for potent inhibitors of breast cancer resistance protein (BCRP), Bioorg. Med. Chem. Lett. 20 (2010) 180-183.

[49] K. Stefan, Untersuchung von Chalkonen und Flavonoiden als BCRP-Inhibitoren, Master Thesis, University of Bonn, 2011.

[50] P. Matsson, G. Englund, G. Ahlin, C.A.S. Bergström, U. Norinder, P. Artursson, A global drug inhibition pattern fort he human ATP-binding cassette transporter breast cancer resistance protein, J. Pharmacol. Exp. Ther. 323 (2007) 19-30.

[51] Y.-L. Ding, Y.-H. Shih, F.-Y. Tsai, M.K. Leong, In silico prediction of inhibition of promiscuous breast cancer resistance protein (BCRP/ABCG2), PLoS One 9 (2014) e90689.

[52] H. Müller I.K. Pajeva, C. Globisch, M. Wiese, Functional assay and structure-activity relationships of new third-generation P-glycoprotein inhibitors, Bioorg. Med. Chem. 16 (2008) 2456–2470.

[53] H. Müller, W. Klinkhammer, C. Globisch, M.U. Kassack, I.K. Pajeva, M. Wiese, New functional assay of P-glycoprotein activity using Hoechst 33342, Bioorg. Med. Chem. 15 (2007) 7470-7479.

[54] W. Klinkhammer, H. Müller, C. Globisch, I.K. Pajeva, M. Wiese, Synthesis and biological evaluation of a small molecule library of 3rd generation multidrug resistance modulators, Bioorg. Med. Chem. 17 (2009) 2524-2535.

[55] A. Telbisz, M. Müller, C. Özvegy-Laczka, L. Homolya, L. Szente, A. Varadi, B. Sarkadi, Membrane cholesterol selectivity modulates the activity of the human ABCG2 multidrug transporter. Biochim. Biophys. Acta 1768 (2007) 2698-2713.

[56] B. Sarkadi, A. Telbisz, ABCG2 transporter assay, WO 2013/128217 A1. September 6, (2013).

[57] *Molecular Operating Environment (MOE)*, 2014.09; Chemical Computing Group Inc., 1010 Sherbooke St. West, Suite #910, Montreal, QC, Canada, H3A 2R7, (2014).

Scheme 1 Reagents and reaction conditions: (i) 8-10 h, 150 °C; (ii) DMF, I_2, K_2CO_3, 70-90 °C, 4-5 h; (iii) $POCl_3$, 9 h, reflux; (iv) 3- or 4-aminoaceophenone, isopropanol, 1-2 h, reflux; (v) substituted benzaldehyde, LiOH, MeOH, microwave (120 W, 100 °C), 30 min.

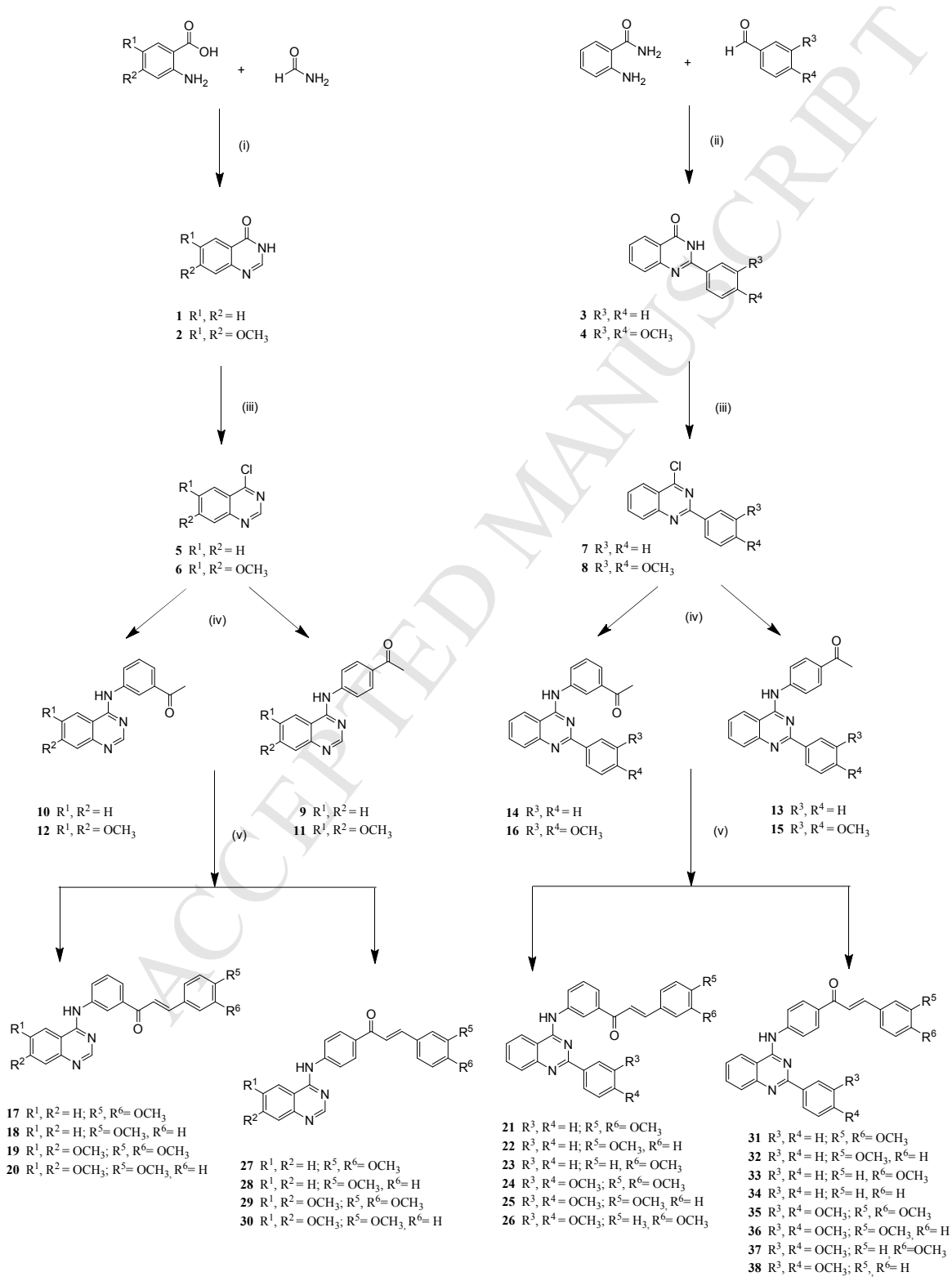

1 R^1, R^2 = H
2 R^1, R^2 = OCH_3

3 R^3, R^4 = H
4 R^3, R^4 = OCH_3

5 R^1, R^2 = H
6 R^1, R^2 = OCH_3

7 R^3, R^4 = H
8 R^3, R^4 = OCH_3

10 R^1, R^2 = H
12 R^1, R^2 = OCH_3

9 R^1, R^2 = H
11 R^1, R^2 = OCH_3

14 R^3, R^4 = H
16 R^3, R^4= OCH_3

13 R^3, R^4 = H
15 R^3, R^4 = OCH_3

17 R^1, R^2 = H; R^5, R^6= OCH_3
18 R^1, R^2 = H; R^5= OCH_3, R^6= H
19 R^1, R^2 = OCH_3; R^5, R^6= OCH_3
20 R^1, R^2 = OCH_3; R^5= OCH_3, R^6= H

27 R^1, R^2 = H; R^5, R^6= OCH_3
28 R^1, R^2 = H; R^5= OCH_3, R^6= H
29 R^1, R^2 = OCH_3; R^5, R^6= OCH_3
30 R^1, R^2 = OCH_3; R^5= OCH_3, R^6= H

21 R^3, R^4 = H; R^5, R^6= OCH_3
22 R^3, R^4 = H; R^5= OCH_3, R^6= H
23 R^3, R^4 = H; R^5= H, R^6= OCH_3
24 R^3, R^4 = OCH_3; R^5, R^6= OCH_3
25 R^3, R^4 = OCH_3; R^5= OCH_3, R^6= H
26 R^3, R^4 = OCH_3; R^5= H_3, R^6= OCH_3

31 R^3, R^4 = H; R^5, R^6= OCH_3
32 R^3, R^4 = H; R^5= OCH_3, R^6= H
33 R^3, R^4 = H; R^5= H, R^6= OCH_3
34 R^3, R^4 = H; R^5= H, R^6= H
35 R^3, R^4 = OCH_3; R^5, R^6= OCH_3
36 R^3, R^4 = OCH_3; R^5= OCH_3, R^6= H
37 R^3, R^4 = OCH_3; R^5= H, R^6=OCH_3
38 R^3, R^4 = OCH_3; R^5, R^6= H

Table 1. Structures and inhibitory potencies of the compounds **17-38** against MDCK II BCRP cells. Data are expressed as mean ± SD (n>3). Ko143 was used as standard.

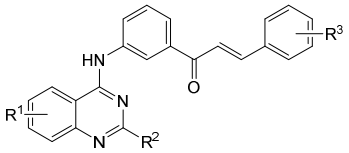

17-26

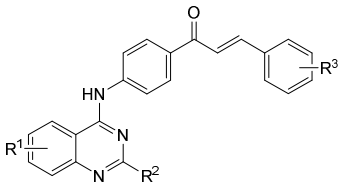

27-38

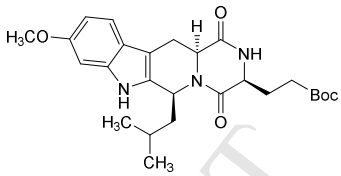

Ko143

Compound	R^1	R^2	R^3	Pheophorbide A assay IC_{50} ± SD [µM]
17	H	H	3,4-OCH_3	1.30 ± 0.12
18	H	H	4-OCH_3	0.89 ± 0.24
19	6,7-OCH_3	H	3,4-OCH_3	1.71 ± 0.07
20	6,7-OCH_3	H	4-OCH_3	0.32 ± 0.02
21	H	C_6H_5	3,4-OCH_3	0.46 ± 0.03
22	H	C_6H_5	4-OCH_3	0.97 ± 0.17
23	H	C_6H_5	3-OCH_3	0.68 ± 0.04
24	H	3,4-$OCH_3C_6H_3$	3,4-OCH_3	0.60 ± 0.04
25	H	3,4-$OCH_3C_6H_3$	4-OCH_3	0.21 ± 0.02
26	H	3,4-$OCH_3C_6H_3$	3-OCH_3	0.31 ± 0.05
27	H	H	3,4-OCH3	0.84 ± 0.16
28	H	H	3-OCH_3	0.68 ± 0.04
29	6,7-OCH_3	H	3,4-OCH_3	1.23 ± 0.17
30	6,7-OCH_3	H	3-OCH_3	0.39 ± 0.01
31	H	C_6H_5	3,4-OCH_3	0.29 ± 0.09
32	H	C_6H_5	3-OCH_3	0.88 ± 0.09

33	H	C_6H_5	4-OCH_3	3.55 ± 0.19
34	H	C_6H_5	H	0.92 ± 0.13
35	H	3,4-$OCH_3C_6H_3$	3,4-OCH_3	0.19 ± 0.02
36	H	3,4-$OCH_3C_6H_3$	3-OCH_3	0.36 ± 0.06
37	H	3,4-$OCH_3C_6H_3$	4-OCH_3	3.13 ± 0.30
38	H	3,4-$OCH_3C_6H_3$	H	1.09 ± 0.13
Ko143				0.24 ± 0.02

Table 2. Inhibitory potencies of selected quinazoline-chalcones on ABCB1 function. For comparison, the inhibition data of the standard inhibitor cyclosporine A is included. Maximum inhibition is the fluorescence plateau level reached in comparison to cyclosporine A. Data is shown as mean ± SD (n = 3).

Compound	Calcein AM assay IC_{50} ± SD [µM]	Max. Inhibition ± SD [%]
17	0.42 ± 0.05	66 ± 4
18	7.08 ± 1.02	N.A.[a)]
19	0.86 ± 0.22	68 ± 13
20	4.15 ± 0.97	N.A.[a)]
24	0.48 ± 0.05	76 ± 8
25	1.29 ± 0.21	70 ± 3
26	8.24 ± 0.07	N.A.[a)]
27	2.34 ± 0.14	61 ± 9
28	5.57 ± 1.31	N.A.[a)]
30	7.55 ± 1.52	N.A.[a)]
31	18.8 ± 5.2	N.A.[a)]
32	32.1 ± 13.2	N.A.[a)]
35	14.9 ± 1.7	N.A.[a)]
36	14.6 ± 4.1	N.A.[a)]
Cyclosporine A	1.41 ± 0.06	100

[a)] N.A.= not analyzable. As no fluorescence plateau was reached at the highest concentration (10 µM) IC_{50}-values were calculated by fixing the top-value to the standard cyclosporine A.

Table 3. Therapeutic ratios of selected compounds were calculated from the IC_{50} values (pheophorbide A assay) and GI_{50} values obtained in MTT cytotoxicity assay with MDCK II and MDCK II BCRP cells.

Compound	IC_{50} in pheophorbide A assay [µM]	GI_{50} (MDCK II BCRP) [µM]	GI_{50} (MDCK II wild-type) [µM]	Therapeutic ratio GI_{50BCRP}/IC_{50}
17	1.30	5.14	3.42	4
19	1.71	11.5	6.14	7
20	0.32	12.7	16.9	40
24	0.60	10.9	12.6	18
25	0.21	13.1	10.3	62
26	0.31	84.7	65.5	273
31	0.29	4.80	3.46	17
35	0.19	92.9	132	489
Ko143	0.24	11.1	10.9	46

Table 4. Therapeutic ratios of selected compounds calculated from the IC_{50} values obtained in the calcein AM assay and GI_{50} values determined in the MTT cytotoxicity assay using A2780 and A2780adr cells.

Compound	**IC_{50} in calcein AM assay [µM]**	**GI_{50} in A2780adr cells [µM]**	**GI_{50} in A2780 cells [µM]**	**Therapeutic ratio GI_{50adr}/IC_{50}**
17	0.42	0.70	0.65	2
19	0.86	1.50	1.35	2
24	0.48	1.71	1.98	4
25	1.29	3.25	4.39	3
Cyclosporine A	1.41	8.63	8.94	6

Table 5. Correlation coefficients of GI_{50}-values determined in the four investigated cell lines.

	MDCK II wt	**MDCK II BCRP**	**A2780 wt**	**A2780 adr**
MDCK II wt	1			
MDCK II BCRP	0.970	1		
A2780 wt	0.846	0.866	1	
A2780 adr	0.832	0.918	0.991	1

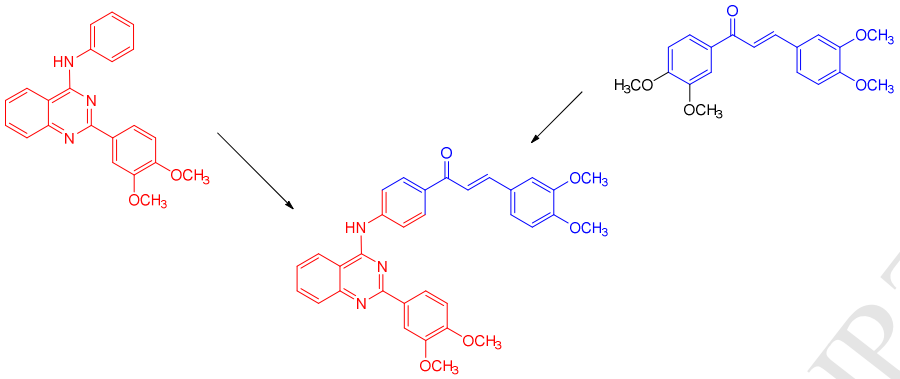

Scaffold	**Pheophorbide A assay IC_{50} ± SD (µM)**
Quinazoline	4.09 ± 1.60
Chalcone	5.12 ± 1.89
Quinazoline-chalcone	0.19 ± 0.02

TOC graphic

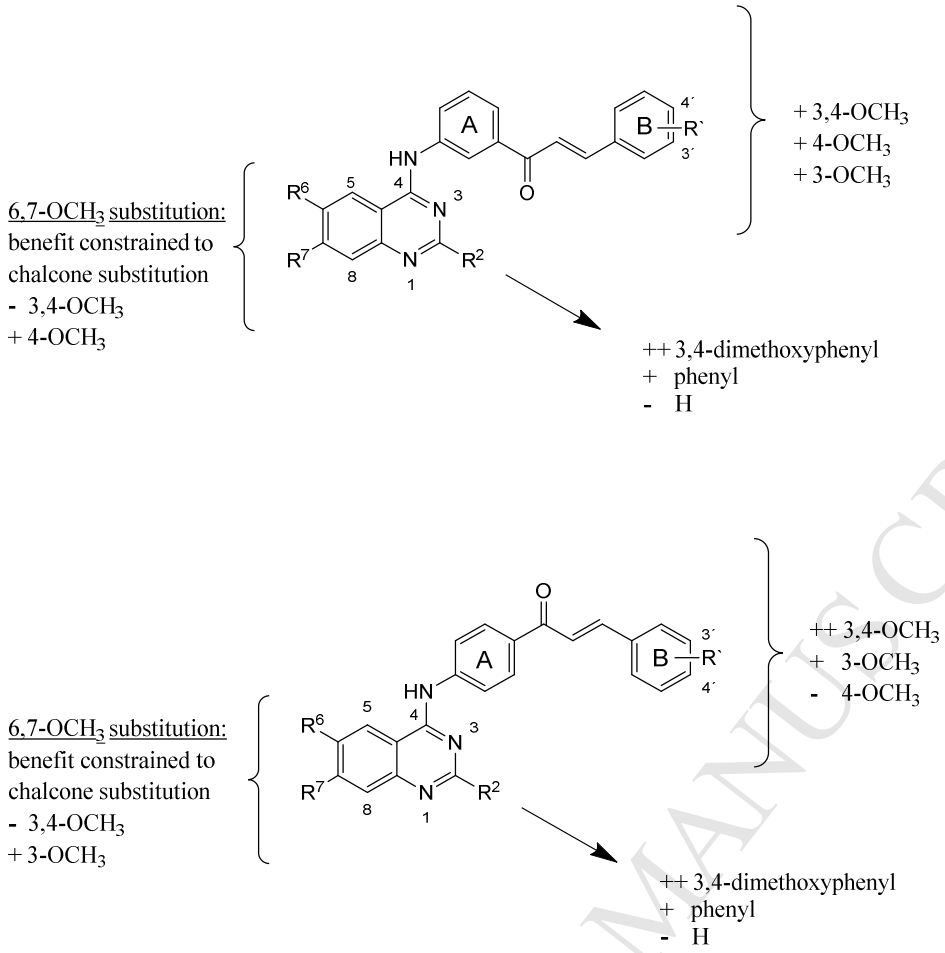

Figure 1. Structural features of the quinazoline-chalcones as ABCG2 inhibitors. ++ very positive, + positive, - negative effect for activity.

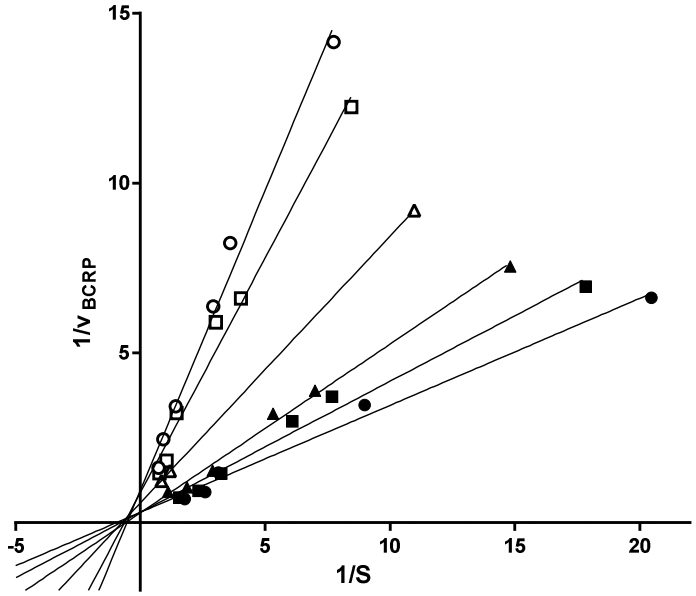

Figure 2. Lineweaver-Burk plot for ABCG2 inhibitor **35** at various concentrations with the ABCG2 substrate pheophorbide A. Inhibitor concentrations used were, 0 µM (closed circles), 0.031 µM (closed squares), 0.1 µM (closed triangles), 0.18 µM (open triangles), 0.31 µM (open squares) and 0.56 µM (open circles).

A

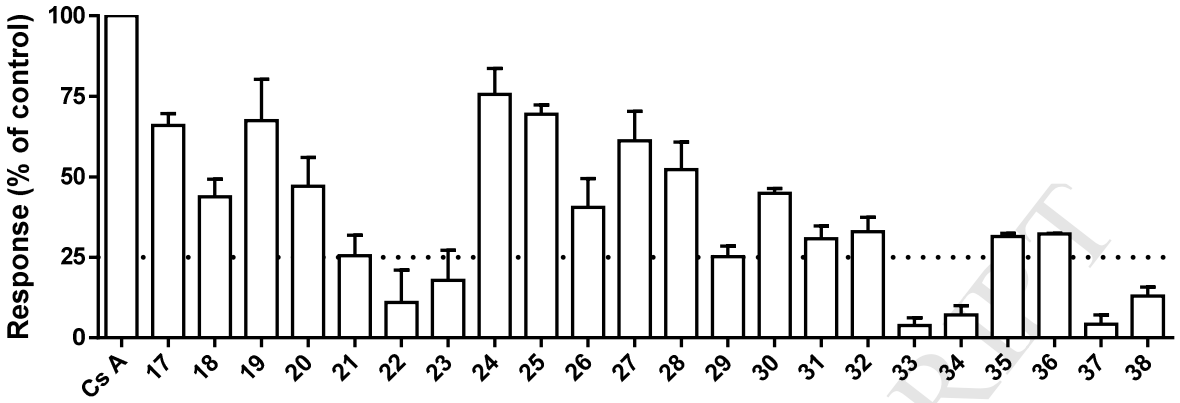

B

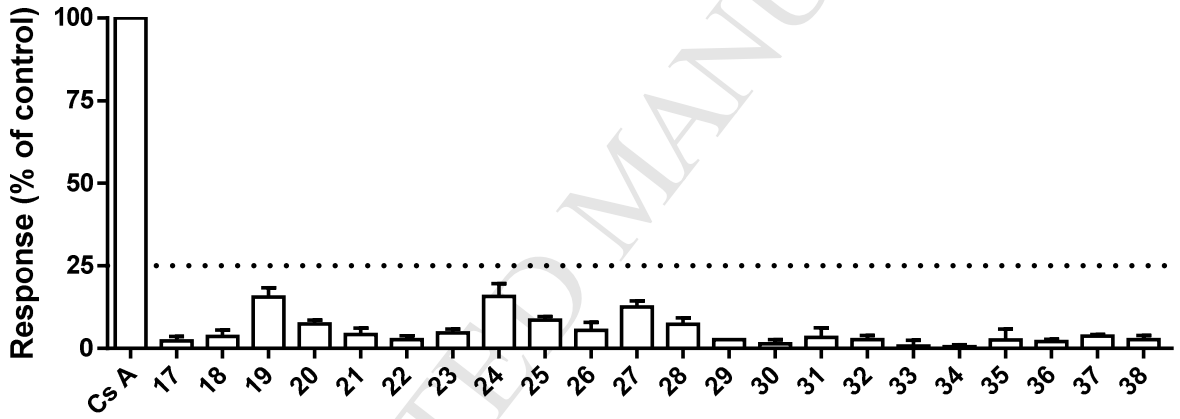

Figure 3. Effects of quinazoline-chalcones at 10 µM concentration on the accumulation of calcein in ABCB1 (A) and ABCC1 (B) overexpressing A2780adr and H69AR cells. Data were normalized by defining the inhibition caused by 10 µM Cyclosporine A (Cs A) as 100 % and are presented as mean ± SD of three independent experiments.

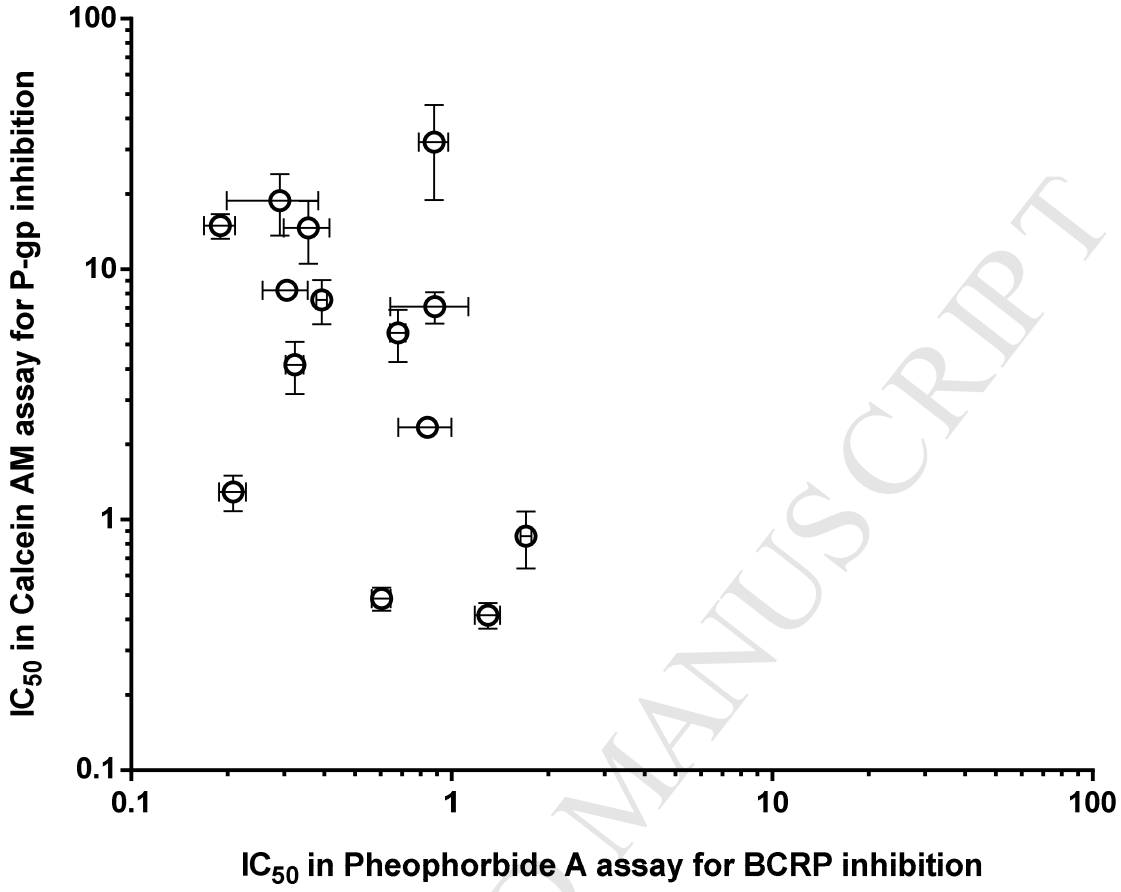

Figure 4. Scatterplot for the IC_{50} values obtained in the calcein AM assay for ABCB1 inhibition and in the pheophorbide A assay for ABCG2 inhibition. Each point indicates mean of IC_{50} values obtained in three independent experiments with the error bars indicating standard deviations.

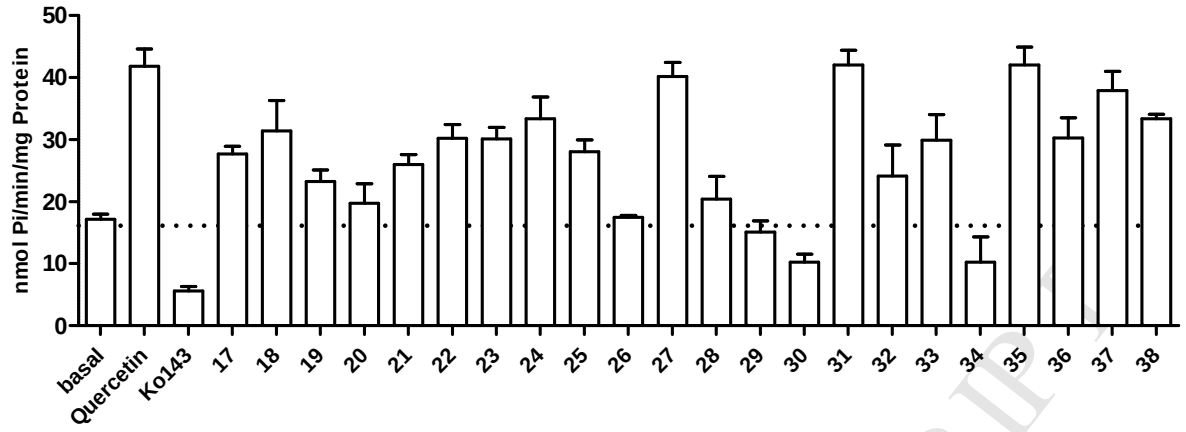

Figure 5. Effects of quinazoline-chalcones on the vanadate sensitive ATPase activity in isolated ABCG2 containing Sf9 membranes at a fixed concentration of 1 µM. Experiments were performed in triplicate. Values are depicted as mean ± SD.

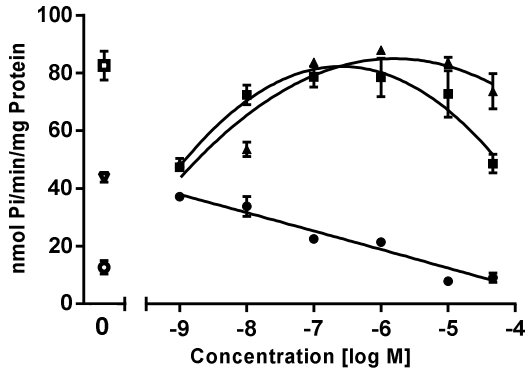

Figure 6. Comparison of the effects of selected compounds on the vanadate sensitive ATPase activity in isolated Sf9 membranes containing ABCG2. Data points of compound **27** (closed triangles) compound **30** (closed circles) and compound **35** (closed squares) depict the values as mean ± SD. Control values show the activity measured in the absence of added compounds (open triangle), in presence of quercetin (open square) as positive control and in presence of Ko143 (open circle) as negative control.

A

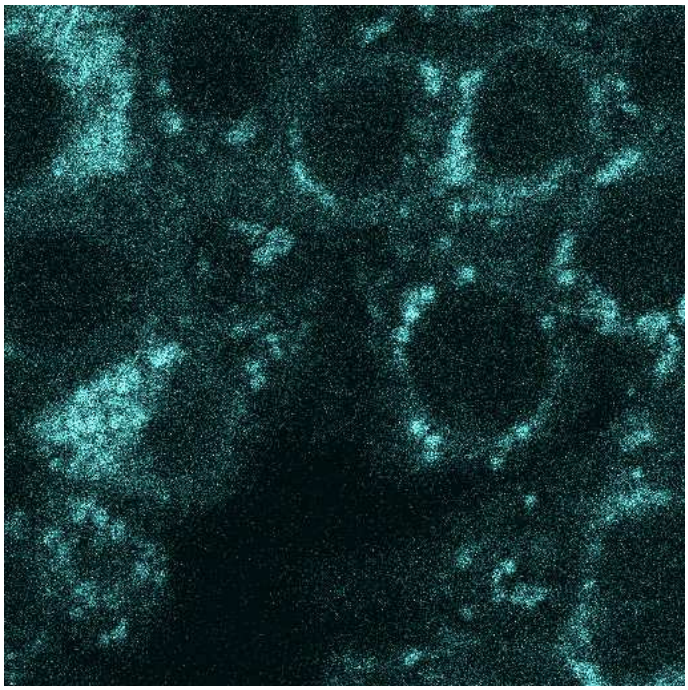

B

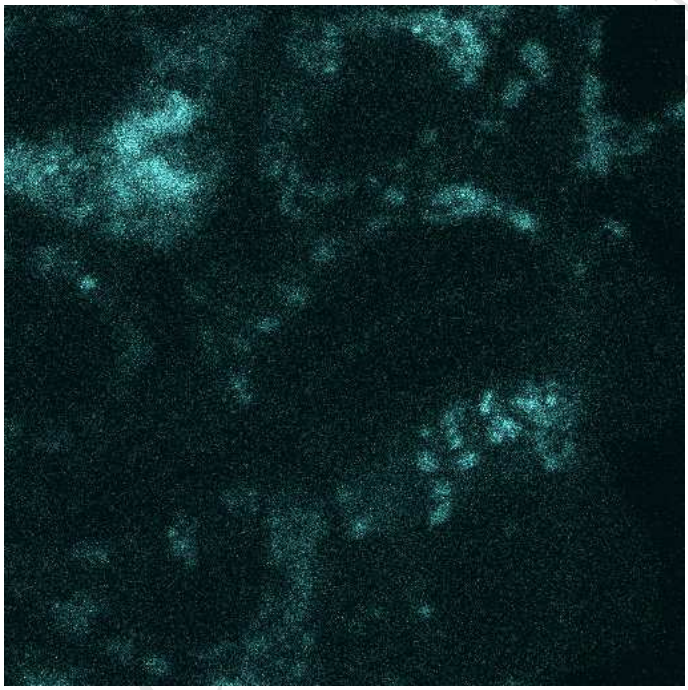

C

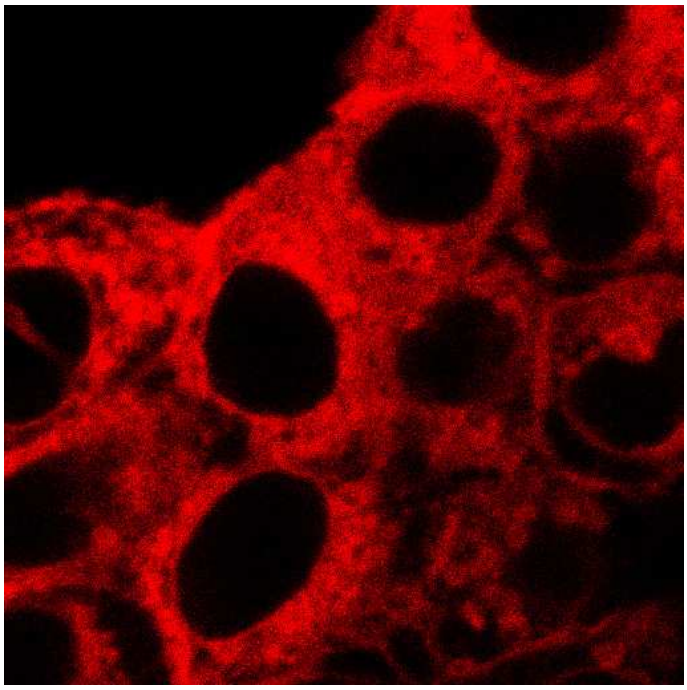

D

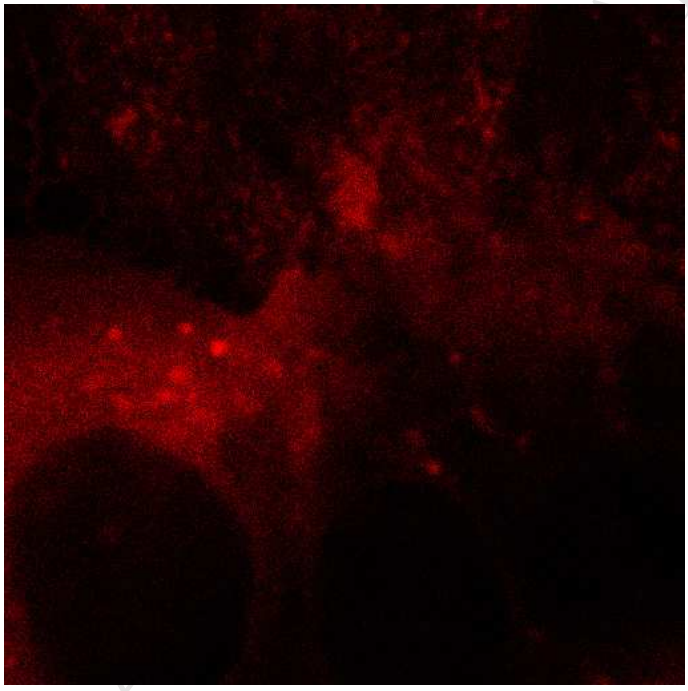

E

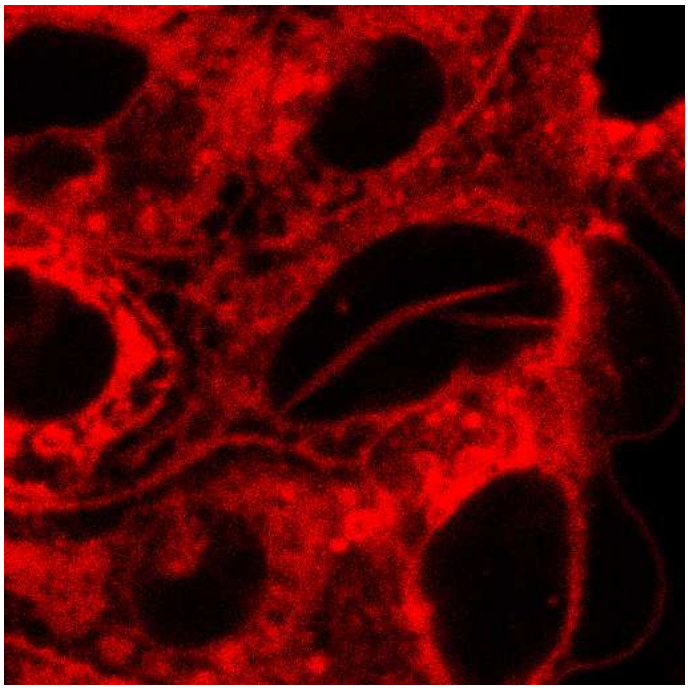

Figure 7. Accumulation of compound **27** in MCF-7 MX cells and parental MCF-7 cells observed by confocal laser scanning microscopy. A: compound **27** in MCF-7 cells; B: in MCF-7 MX cells; C: Pheophorbide A in MCF-7 cells; D: Pheophorbide A in MCF-7 MX cells; E: Pheophorbide A in presence of compound **27** in MCF-7 MX cells.

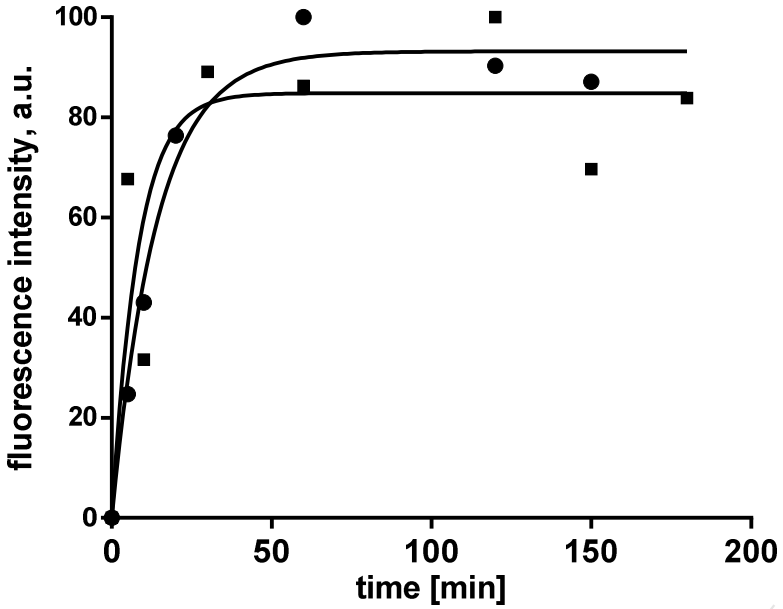

Figure 8. Intracellular fluorescence concentrations of compound **27** measured at regular time intervals in MCF-7 MX (closed circles) and parental MCF-7 cells (closed squares). Data is depicted as mean ± SD.

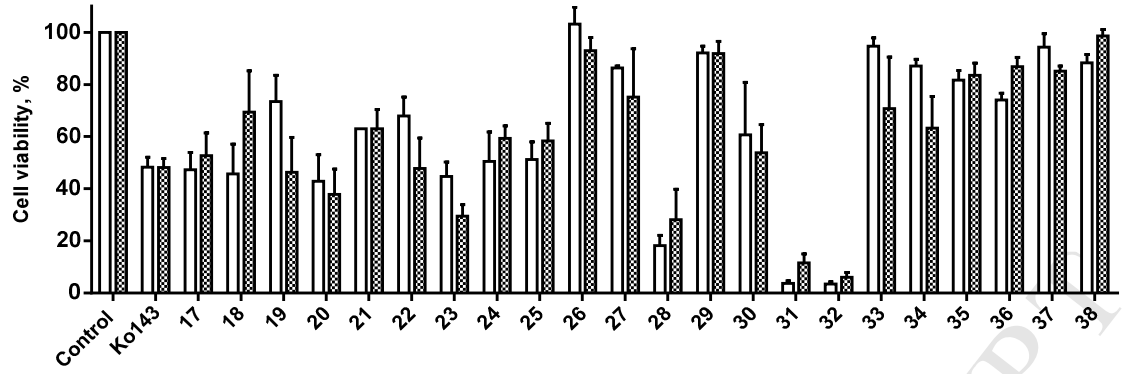

Figure 9. Bar chart illustrating the influence of the studied quinazoline-chalcones (10 µM) on the cell viability of MDCK II BCRP (white) and MDCK II wild type cells (dark). To determine the cell viability the MTT assay was used. Data were normalized by defining the control as 100 %.

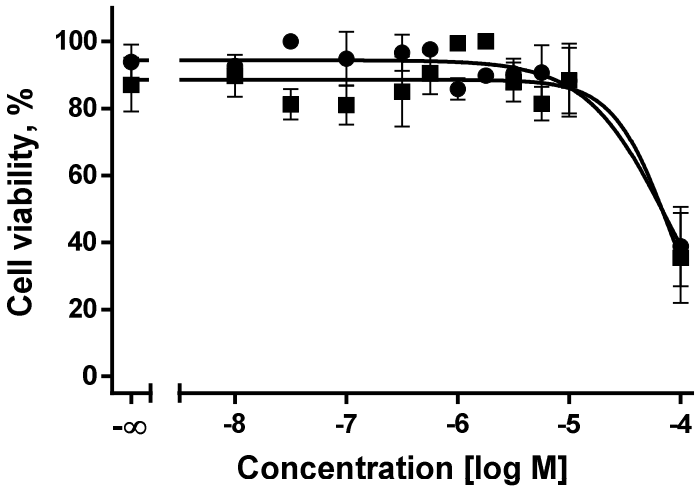

Figure 10. Concentration-response curve of compound **35** obtained in the MTT assay using the MDCK II BCRP (closed circles) and MDCK II wild type (closed squares) cells after a 72 h incubation period (GI_{50} = 87 µM). Data is shown as mean ± SD.

A

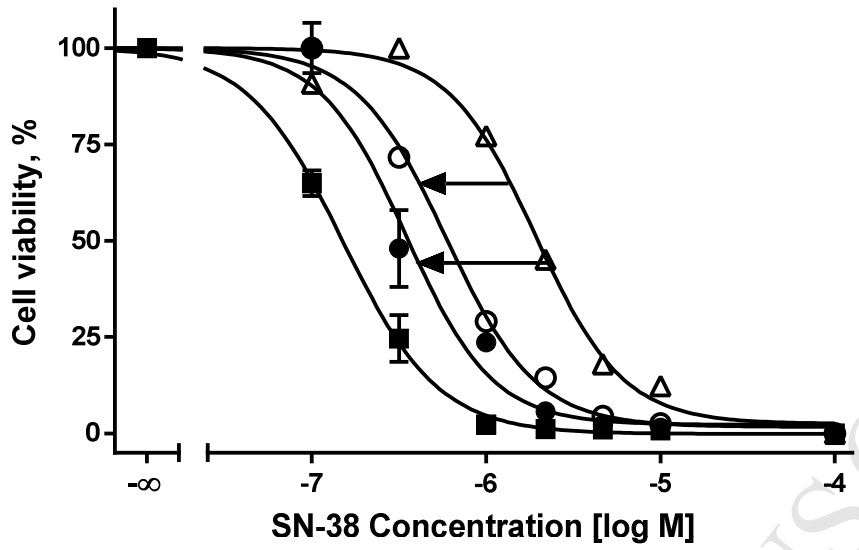

B

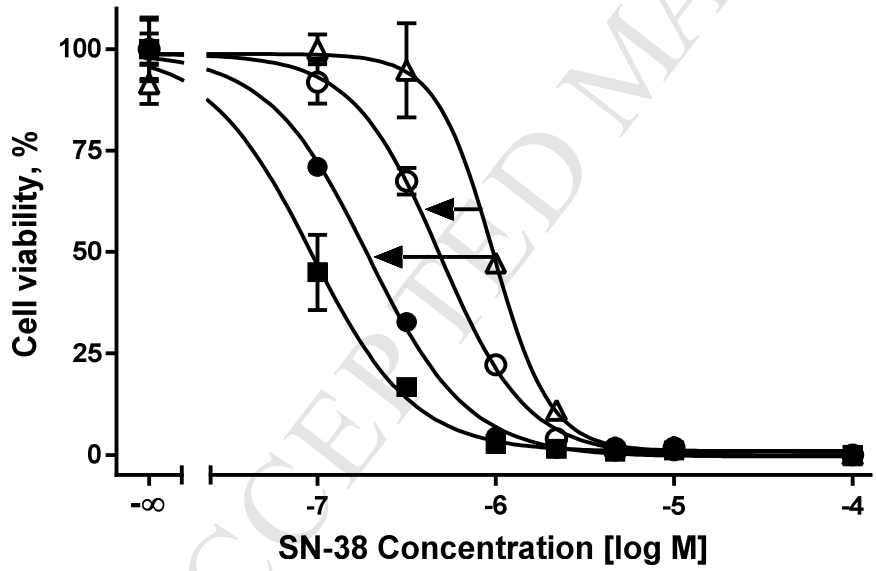

Figure 11. Representative shifts in dose-response curves of SN-38 cytotoxicity. Panel A and B depict the effect of compound **35** (A) and Ko143 (B) on SN-38 cytotoxicity. Arrows indicate dose dependent sensitization of MDCK II BCRP cells towards SN-38. Both compounds were investigated at 0.01 µM (open circles) and 0.1 µM (closed circles) concentrations. ABCG2 overexpressing MDCK II cells without inhibitor (open triangles) are more resistant than sensitive wild-type MDCK II cells (closed squares).

A

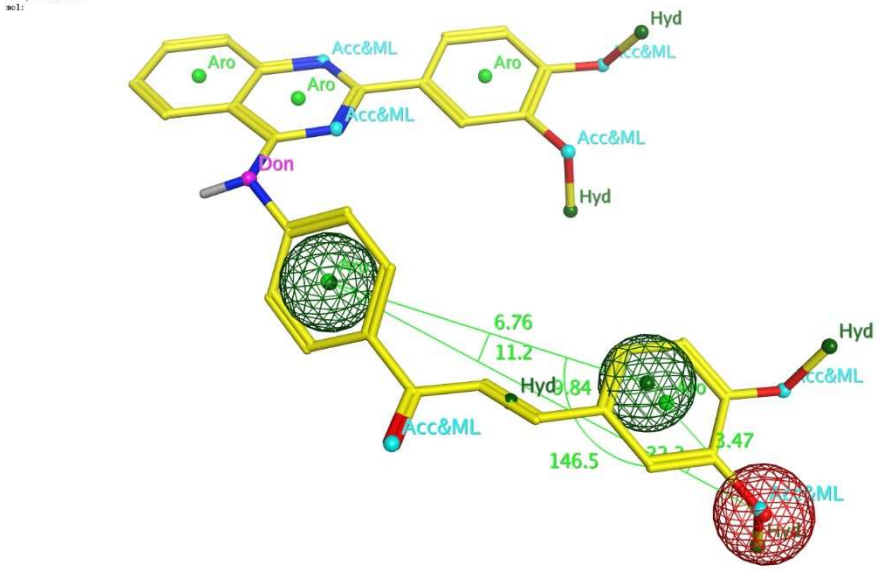

B

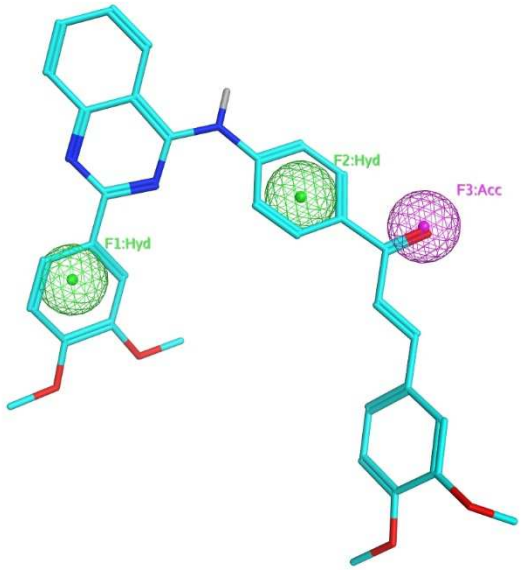

Figure 12. Flexible overlay of compound **35** on the pharmacophore model derived by Matsson et al.[50] Panel A shows the defined pharmacophoric features and their distances together with a typical superposition involving the chalcone substructure of the compounds only. In panel B the second type of overlay is presented, involving the 2-phenyl ring of the quinazoline part, the 4-anilino group and the carbonyl group of the chalcone.

Highlights:

- Combination of quinazoline and chalcone scaffolds to heterodimeric inhibitors
- Quinazoline-chalcones are potent inhibitors of ABCG2
- Most potent compound was found to be selective, non-toxic and able to reverse MDR
- Stimulate ATPase activity without being transported
- Three compounds show dual inhibitory behavior